CHALMERS

Reconfigurable Bioimpedance Spectrometer for the Evaluation of Impedance Estimation Methods Suitable for Spectroscopy Measurements
Master of Science Thesis in Biomedical Engineering

ZELEALEM KEBKAB KASSAYE

Reconfigurable Bioimpedance Spectrometer for the Evaluation of Impedance Estimation Methods Suitable for Spectroscopy Measurements

ZELEALEM KEBKAB KASSAYE

Department of Signals and Systems
Division of Biomedical Engineering
CHALMERS UNIVERSITY OF TECHNOLOGY
Telephone +46(0)735744054

Supervisor:
Fernando Seoane
University of Borås
School of Engineering
SE-501 90 Borås
Sweden
Telephone +46(0) 334354008

Examiner:
Bo Håkansson
Chalmers University of Technology
SE-412 96 Göteborg
Sweden
Telephone +46(0) 317721807

Dedicated to

Our late mother Ejigayehu Mekuria

Abstract

The measurement of electrical bioimpedance deals with the measurement of the opposition to the flow of charges exhibited by a biological material when an electrical stimulus is applied. The impedance estimation implemented in an impedance meter is a paramount key functional blocks influencing in the measurement performance and application of the measurement device. In this work a configurable bioimpedance measurement system has been implemented using the NI USB-6218 Data Acquisition board and LabVIEW development environment. The implemented system allows the implementation of different impedance estimation methods and tests their performance. To show the intended functionality two different impedance estimation methods have been implemented: Digital Sine Correlation and Digital Deconvolution through Total Least Squares. The performances of both systems have been validated with 2R1C circuits. The multisine excitation implemented with two NI USB-6218 units produce a time delay that required signal synchronization prior the application of digital deconvolution. The measurement results show that is possible to produce multifrequency bioimpedance measurements with both approaches well using frequency sweeping or multisine excitation.

Key words: Electrical bioimpedance Spectroscopy, Total Least Square, Digital Sine Correlation, Digital Deconvolution NI USB-6218 Data Acquisition Device, LabVIEW.

Acknowledgments

List of Figures

List of Tables

List of Acronyms

AC	Alternating current
DAQ	Data Acquisition
DC	Direct Current
DSC	Digital Sine Correlation
EBI	Electrical Bioimpedance
EBS	Electrical Bioimpedance Spectroscopy
ECW	Extracellular Water
FFT	Fast Fourier Transform
ICW	Intracellular Water
LabVIEW	Laboratory Virtual Instrument Engineering Workbench
LS	Least Square
NI	National Instruments
PFI	Programmable Function Interface
SVD	Singular Value Decomposition
TLS	Total Least Square
VCCS	Voltage Controlled Current Source
Z	Impedance

Table of Contents

Chapter 1. **Introduction**

1.1   Introduction

The opposition experienced when an electrical charges flow through a biological material is known as Electrical Bioimpedance (EBI). These biological materials do not only exhibit an opposition to the flow of electrical charges but can store electrical energy, the charges and field also experience a phase shift. Therefore, EBI measurements must be represented as a complex number.

The measurement of EBI is a relatively simple and requires two or more electrodes. The measurement can be use to asses in the subject's blood flow, cardiac activity, respiration activity, bladder, blood and kidney volumes and etc (Sverre Grimnes 2006). When the EBI measurements are taken at various frequency points it is called EBI spectroscopy. Measuring the impedance in a range of frequencies gives a spectrum that can easily show the relationship between impedance and frequency. This relationship can give an indication about the status of the biological tissue under study (Zilico 2012). The applications of the measurements of EBI spectroscopy include the assessment of intracellular water (ICW) and extracellular water (ECW) conditions (M.Tengvall 2009).Therefore several applications can be built up based on performance of EBI measurements and it is a non-invasive method of measurement of physiological conditions.

1.2   Motivation

For trained technician, a measurement of an EBI is a forward task to perform and it is non-invasive. Even if EBI spectroscopy is simple to perform its measurement performance and applications are dependent on the different functional building units of it. The impedance estimation block is one of the main functional blocks of EBI spectroscopy. The others include electrodes, voltage and current measurement blocks. The study of the building blocks of EBI measurement systems and setups is helpful in having a good quality measurement result.

Constructing EBI measurement setup that can be configurable is a need to study the influence that each of the building blocks creating to the measurement results. Designing an analog current source and using LabVIEW development environment and NI USB-6218 multifunction data acquisition card (DAQ) allow to study how the building blocks mainly the impedance estimation block is affecting the overall measurement result. The impedance estimation block can easily be configured as the study's need in such custom made EBI spectrometer. Its effect on the measurement results can be shown by doing different configuration at different setups like number of sample used in the estimation and the use of different voltage or current measurement configuration.NI USB-6218 is USB powered device hence can be driven by portable computer battery power. This enhances the electrical safety regarding applications on human beings.

1.3   Goal
The goal of this work is to implement a bioimpedance spectroscopy meter that can work at a single and multi-frequency that allows test the performance and influence on the measurements of different alternatives to the functional blocks and especially for different impedance estimation approaches. Commercially available meters are made application specific and do not allow modifying them and sometimes making impossible to use in experimental environments.
There are different impedance estimation approaches; some of them are Digital Sine Correlation (DSC), Digital Deconvolution by Total Least Square (TLS) and Fast Fourier Transform (FFT) methods. The performance comparison of the two EBI measurement estimation approaches, DSC of frequency sweeping application and digital convolution by TLS of multifrequency application is used to evaluate the correct operation of the implemented EBI spectroscopy meter.

1.4   Work done
In this thesis the executed work includes design and analog electronic implementation of a Voltage Controlled Current Source (VCCS), implementation of DSC using LabVIEW and measurement of an equivalent electrical circuit of cells using 2R1C parallel model. Calibration is done on a known set of 2R1C parallel model. Measurements are taken with different sets of 2R1C parallel model using the calibrated setup. The raw measurements, theoretical values and calibrated measurements of a 2R1C parallel model given as result of this work.
The multifrequency estimation of bioimpedance is implemented using the TLS method and used Singular Value Decomposition (SVD) as a computational tool. An analog circuit of summing amplifier in an inverted operational amplifier configuration is used as a VCCS and TLS is implemented using the LabVIEW on NI USB-6218 DAQ card. The raw measurements, theoretical values and the calibrated measurements of a 2R1C parallel model given as a result of this work.

1.5   Structure of the Report
The sections that are contained in this thesis report are six chapters, a bibliography and an appendix section. Chapter one Introduction contains the introduction, motivation, goal and work done on this thesis. Additionally parts that are not covered on this work are listed in out of scope part of this chapter. Chapter two of this work, Background-Bioimpedance discusses about the basic concepts of electrical bioimpdance, the electrical properties of biological a tissues, equivalent electrical circuit of a cell and bioimpedance measurement systems including electrode configuration. Chapter three, Methods and Materials, covers the methods and materials used in measurement of EBI with their implementation in this work. Current source types, data acquisition and analysis hardware and the measurement setup are the other things that are discussed in chapter three.   Chapter four Results, contains the EBI measurement results that are taken during this work. Chapter five Discussion, discuses the EBI measurement results of the work. The last chapter ,Chapter six Conclusion and Future work, puts the conclusion that is drawn from the work and gives the possible further extensions of this work.

In the Appendix section of this work, the bibliography used and the specification summary of the DAQ are given.

1.6 Out of Scope

In this work the following points are not studied

- To test the performance of the implemented EBI spectrometer in human subjects is not included.

- Comparisons of different measurement parameters that affect the impedance estimation are not studied.

- Any comparison of the obtained measurement performance with commercially available devices is not studied.

Chapter 2. **Background-Bioimpedance**

2.1 Introduction to Bioimpedance

The electric impedance is an opposition that a material present when excited by an electrical stimulus like alternating current (AC) of particular frequency. The electrical impedance (Z) is given by a complex relation that has two components, the first real part is denoted by R which is resistive component of the impedance and the imaginary part is denoted by X which is the reactive component of the impedance and shown as follows

$$Z = R + jX \ [\Omega]$$

$$Z = |Z| \angle \theta$$

Where $|Z| = \sqrt{R^2 + X^2} \ \ \theta = \tan^{-1}\left(\frac{X}{R}\right)$

$$R = |Z| \ \cos\theta \text{ and } X = |Z| \sin\theta$$

Equation 2.1

This can be given in a graphical representation in a complex plane as below.
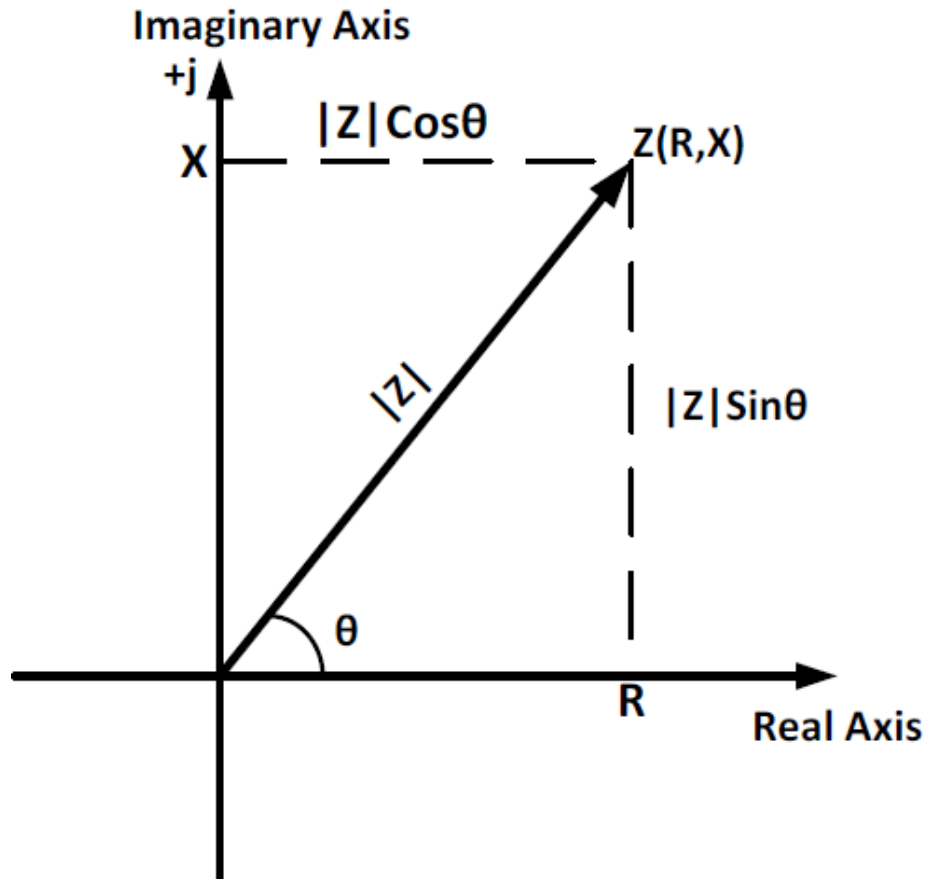
Figure 2-1 Complex Representation of Impedance.

As a material, biological tissues have different types of properties that include their electrical behavior. EBI is one of its electrical properties (Tabuenca 2009). EBI is the resistance that is created when a biological tissue is subjected to an electrical excitation of current or voltage and it is dependent on the value of the frequency of excitation of the current or voltage. The measurement of EBI to assess and study the behavior of the biological tissues as it is subjected to an AC has a long lasting history (Patterson 2000).

2.2 Electrical Properties of Biological Tissues

A biological tissue is made up of cells that perform a particular function in the organism's body. The cells building these tissues are suspended on a fluid called extracellular (outside cell) fluid. It is composed mainly of interstitial (between cells) fluid (about 80%) and the remaining part is composed of blood plasma (about 20%), a liquid part of the blood. The cells also have fluid inside them - intracellular (inside cell) fluid or cytosol of the cell in which the organelles of the cell are suspended. In these fluids electrolytes like Na^+, K^+, Cl^-, Ca^{2+} and proteins occur. These electrolytes are free to move in the fluids that they are predominantly found and as well to the other fluid. The concentration and presence of each of the electrolytes in the extracellular fluid is different from that of the intracellular fluid (Gerard J. Tortora 2007).

Table 2-1 Electrolyte and protein anion concentration (Gerard J. Tortora 2007).

Electrolyte/protein anion	Concentration(mEq/lit)	
	Extracellular fluid	Intracellular fluid
Na^+	142	10
K^+	4	140
Cl^-	100	3
Ca^{2+}	5	0.2
Protein anions	20	50

Unlike metal conductors, the free moving ions in both fluids are serving as charge carriers which in turn are responsible in creating the electrical conductive property of biological tissues.

2.2.1 Plasma Membrane

Plasma membrane is a life line of the cell; if it is destroyed a cell will die. Plasma membrane encloses the cell and it makes a compartment for the extracellular fluid and intracellular fluid.

The plasma membrane is built from phospholipids- lipids that have phosphors. It is constructed in such a way that the two phospholipids layers come into back to back forming a lipid bilayer (Gerard J. Tortora 2007). The plasma membrane has a resistivity of approximately $100\Omega/cm^2$ and $1\mu F/cm^2$ of capacitance per unit area and shows a property of a capacitor which varies as the value of the frequency of the excitation AC changes. The intracellular fluid which is an ionic solution has around$100\Omega/cm$ and extracellular fluid has approximately $60\Omega/cm$ (Tabuenca 2009).

2.3   Equivalent Electrical Circuit of a Cell

Biological tissues are formed from a number of cells that have the same type of function in the organism's body. Its properties are derived from the cumulative properties of the cells that are the building block of the biological tissue. Having an equivalent electrical circuitry representation of a Cell is basic tool in studying their electrical property especially their Bioimpedance property (Seoane 2007). This equivalent electrical circuitry has a simple representation of the extracellular fluid, intracellular fluid and the plasma membrane with a combination of resistors and capacitors.

A simple way of giving the equivalent electrical circuitry model is called Fricke's circuit. The Fricke's circuit put the circuit model of cells as the two fluids in the biological tissue i.e. extracellular and intracellular fluids, in parallel and the barrier between them i.e. the plasma membrane as a capacitor which is in series with the intracellular fluid (Ursula G. Kyle 2004).
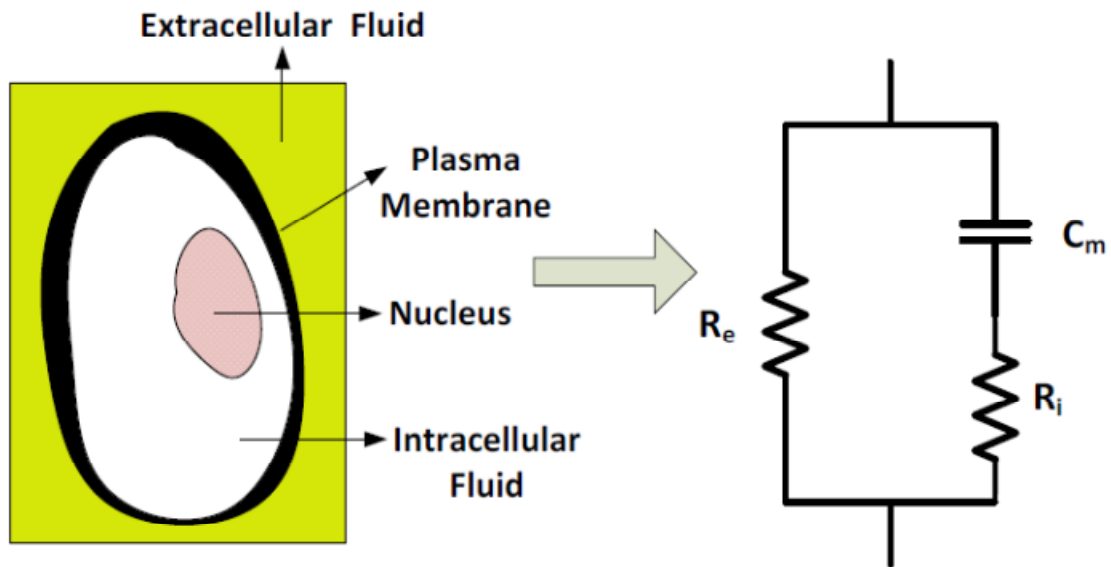
Figure 2-2 Structure of a cell with Intra- and Extracellular Fluid, plasma membrane Nucleus and its Equivalent Electrical Circuit.

The equivalent impedance of the model is calculated easily from the given components R_e, R_i, and the impedance value of the capacitor is given by X_c and is equal to:

$$X_c = -j \; \frac{1}{2\pi f C} \; [\Omega]$$

Equation 2.2

Then R_i and X_c are in series and they become

$$R_i + X_c = R_i + \frac{1}{j2\pi f C}$$

Equation 2.3

and on the other electrical branch of the model R_e is in parallel with Equation 2.3. This gives the equivalent impedance of the model as follows

$$Z = R_e||(R_i + X_c) = \frac{R_e \times (R_i + \frac{1}{j2\pi fC})}{R_e + (R_i + \frac{1}{j2\pi fC})}$$

$$Z = \frac{\frac{R_e \times (R_i \times j2\pi fC + 1)}{j2\pi fC}}{\frac{(R_e \times j2\pi fC + R_i \times j2\pi fC + 1)}{j2\pi fC}}$$

$$Z = \frac{R_e \times R_i \times j2\pi fC + R_e}{(R_e \times j2\pi fC + R_i \times j2\pi fC + 1)}$$

$$Z = \frac{R_e \times (1 + R_i \times j2\pi fC)}{j2\pi fC(R_e + R_i) + 1}$$

Rearranging and substituting Equation 2.4 into the above equation

$$\omega = 2\pi f$$

<div align="right">Equation 2.4</div>

is resulting the equivalent impedance of the simple cell model for biological tissues. The final equation is given by

$$Z = \frac{R_e(1 + R_i j\omega C)}{1 + j\omega C(R_e + R_i)}$$

<div align="right">Equation 2.5</div>

Equation 2.5 is able to show the behavior of the equivalent impedance at low or zero frequency and at high or infinite frequency. At lower frequency ($\omega = 0$), the plasma membrane hinders the excitation AC from passing through it and it makes its way across the extracellular fluid outside of the cells. This results the equivalent impedance to become (Ursula G. Kyle 2004).

$$Z_0 = R_e$$

At higher frequencies ($\omega = \infty$), the plasma membrane that is given by C_m in the model behaves as a perfect conductor and its impedance which is given in Equation 2.2 is becomes zero and the respective equivalent impedance becomes a parallel combination of the R_e and R_i which is the combination of the extracellular and intracellular fluids and is given as below (Ursula G. Kyle 2004).

$$Z_\infty = \frac{R_e \times R_i}{R_e + R_i}$$

The above phenomenon is illustrated in the following figure that is showing how low frequency and high frequency signals interact with cells and fluids inside and outside of them.
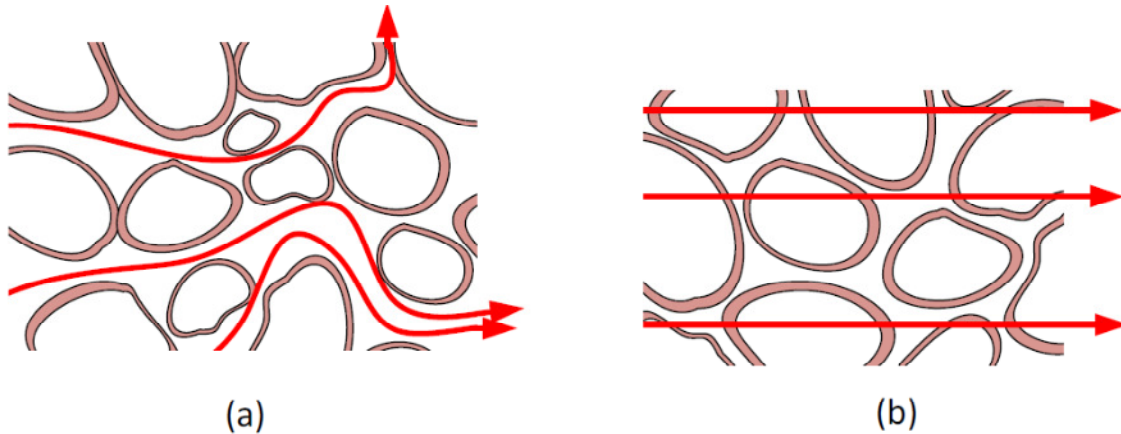
Figure 2-3 Injected Current Path at (a) Low Frequency and (b) High Frequency in Biological Tissues.

2.4   Dispersion of a Biological Tissue-Frequency Dependency

When the permittivity of material changes as a function of the frequency of the exciting stimulus, the material is called dispersive medium. Biological tissues show this behavior and can put under this category of materials (Seoane 2007). As frequency of the excitation AC increases, the permittivity of the biological tissue shows a decrease where as conductivity increases. There are windows of dispersion that were revealed and given the names α, β, γ- dispersion by H.P. Schwan (1963). These windows can be seen when plotting the spectrum of permittivity or conductivity of biological tissues.
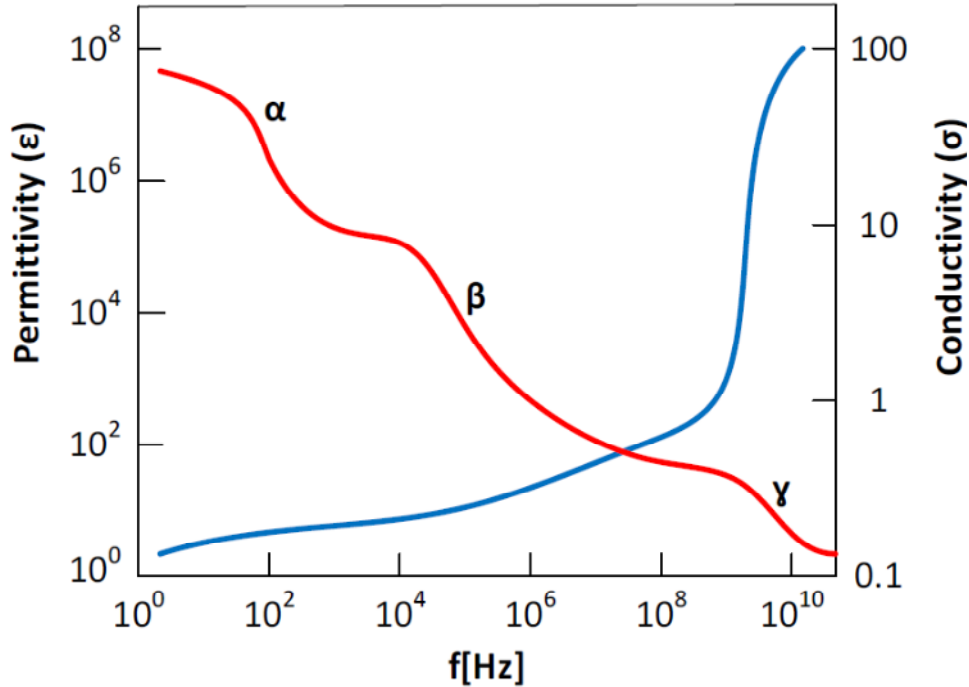
Figure 2-4 Regions of Dispersion, Frequency verses Permittivity and Conductivity.

The α – dispersion is present in a frequency range of mHz to kHz. In the range of 1 kHz to 100MHz, the β – dispersion is the predominant dispersion. The range 0.1 GHz to 100 GHz is dedicated to the γ – dispersion (Sverre Grimnes 2008). But it is not possible to exactly demarcate each windows as they are continues one into the other window (P.Schwan 2001).

2.5   Bioimpedance Measurement

Measurement of the impedance Z of a given tissue can be performed using two different approaches. Applying a controlled amount of AC current to the tissue and measuring the response AC voltage is the first approach and the most common way of measurement (R. Gordon 2005).The second methodology is done by applying AC Voltage to the tissue and measuring the response AC current.

At the first approach the excitation AC current I and the response AC voltage are known from the measurement setup. The excitation AC voltage V and the response AC current are known in the second approach. From both the approaches the known values are enough to derive the complex impedance of the tissue by applying the Ohm's law. The Ohm's law is given by:

$$Z = \frac{V}{I} \ [\Omega]$$

Where Z = R + jX

Equation 2.6

When the excitation is performed, electrical safety has to be given a great consideration since the measurements done on living tissue. The quantities that one has to consider include the value of the excitation current and current density. Direct current (DC) excitation is not absolutely favorable to do impedance measurement due to its ability in creating charge deposition the

9

biological tissue. If the magnitude of the electrical stimulus is very large, this can affect the tissues in contact (Seoane 2007).

2.5.1   Electrode Arrangement

During measurement of an EBI there are contact sites on the biological material that the known and controlled current or voltage injected and the respective response voltage or current measurement took place. At these particular sites there has to be some sort of interfacing material that can make a transfer in-between the measurement instrumentation and the biological tissue. The interfacing elements are known as electrodes. These electrodes are places where the exchange of electronic charge carriers of the measurement system to ionic charge carriers of the biological tissues takes place (Sverre Grimnes 2006). Most often in EBI measurements, there are three different configurations of electrodes use: two, three and four electrode systems. Below only two configurations described further i.e. two and four electrode systems.

2.5.1.1   Two Electrodes System

The two electrodes system applies two electrodes as injecting and measuring interfaces as the same time. The flaw of this electrode configuration is what with such topology leads to measure not only the impedance of the biological tissue but impedance of the skin-electrode. Since the value of such impedance is several order larger than the EBI of target, the final impedance measurement will contain the target EBI masked by the impedance of the interface.
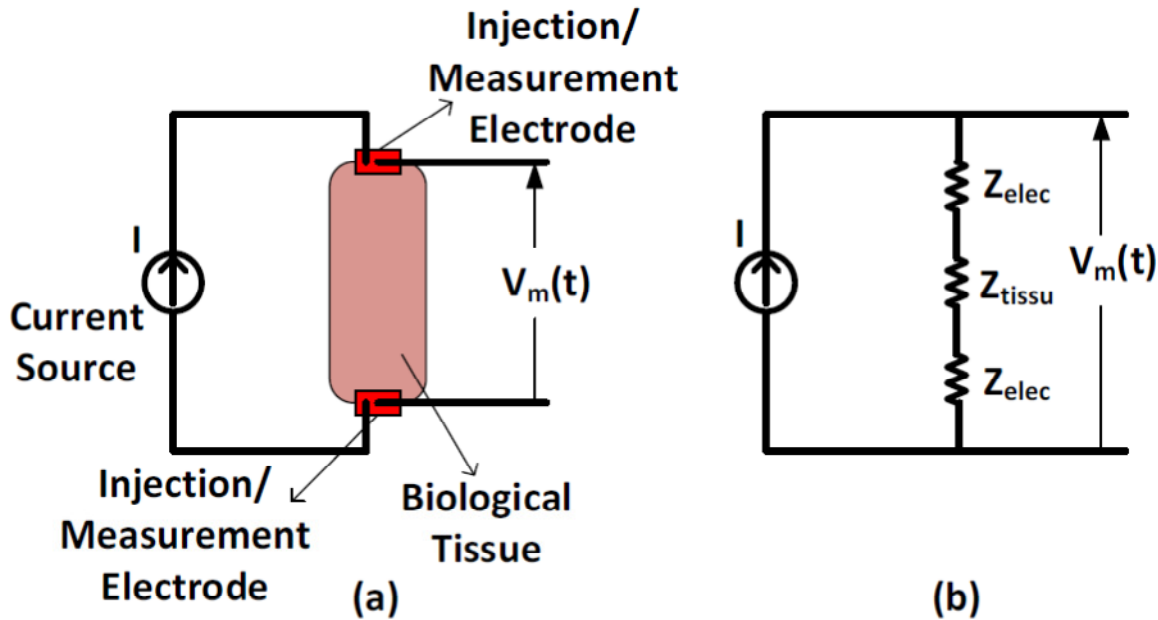
Figure 2-5 Bioimpedance Measurements system (a) Two Electrode Setup and (b) Its Equivalent Electrical Circuit.

2.5.1.2   Four Electrodes System

The four electrodes system is applied by using two electrodes for excitation of the biological tissue and the other two serve as a measurement electrodes. The site of application of each pair of injection and measurement electrodes are distinct. The application of four electrodes setup removes the main inconvenience introduced by the use of two-electrode system. Due to such

advantage , four electrodes approach is most often the choice of use (Seoane 2007). The use of four-electrode configuration is critical when spectroscopy measurements are performed, when the two-electrode configuration is not a valid option.
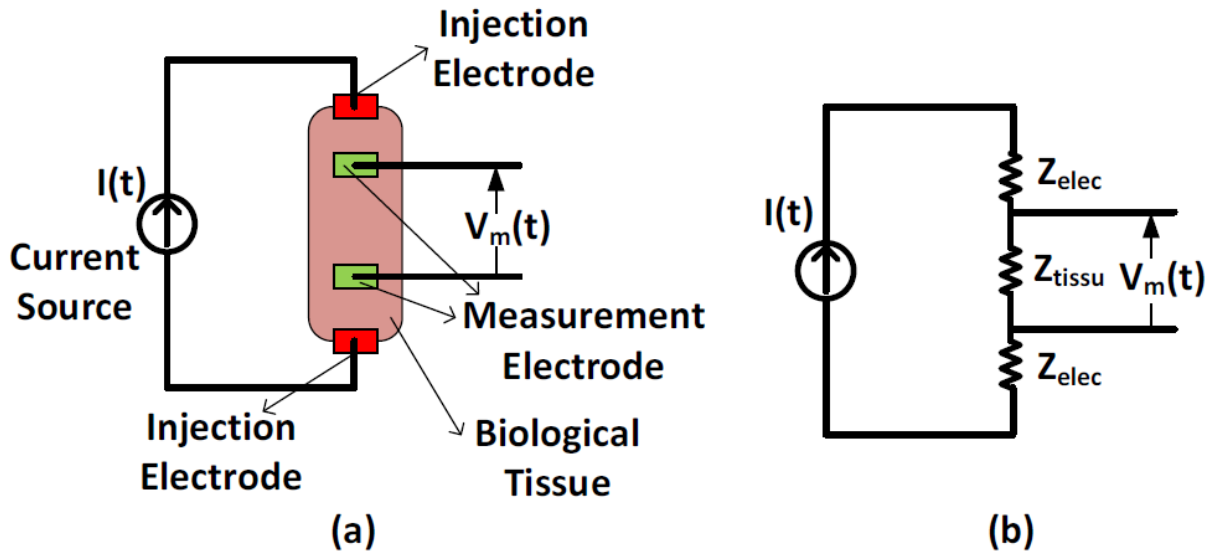
Figure 2-6 Bioimpedance Measurements system (a) Four Electrode Setup and (b) its Equivalent Electrical Circuit.

Chapter 3. **Materials and Methods**

3.1   **Materials and Methods**

In this section of this work the materials and methods used and applied in this thesis work are discussed. A Voltage Controlled Current Source (VCCS) and the National Instruments Data Acquisition Device (DAQ) NI USB-6218 are used for the implementation of this work. The graphic programming software Laboratory Virtual Instrument Engineering Workbench (LabVIEW) is mainly applied in generating, acquiring, processing and analyzing of the data.
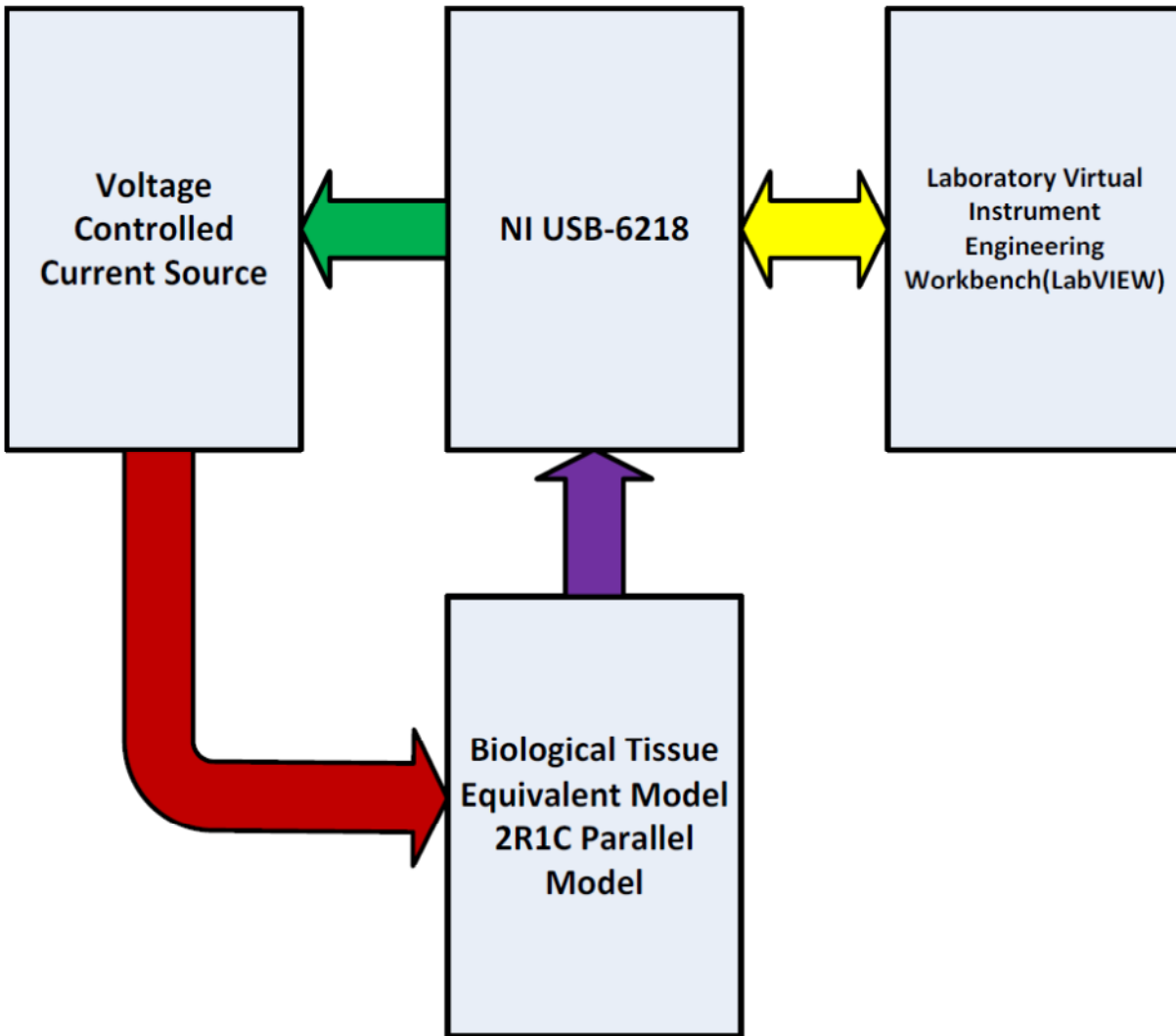
Figure 3-1 Block Diagram of Components and their connections.

3.2   **Current Source**

A conventional method of performing Electrical Bioimpedance measurement is by injecting an AC current with constant magnitude to the biological tissue under investigation and measuring the response AC voltage across it. The current source for the stimulation of biological tissues is a basic functional part of an Electrical Bioimpedance measurement system. Implementing a

current source which is able to deliver a constant magnitude of current that it generates to the electrodes at the surface of the biological tissue is the main requirement of its design. This can be addressed by designing a current source that has large output impedance. Getting infinite output impedance is an ideal assumption in designing the current source. It can result an equal amount of injected current at the injection site with the generated current whatever that the value of impedance of the biological tissue (Seoane 2007). The output impedance of the current source is also dependent on the frequency of the measurement system, as frequency increases it decreases. Because of this dependency, the output impedance of the current source limit the frequency band in which the Electrical Bioimpedance system works and the value of the impedance of the biological tissue under investigation (Seoane et al. 2011) .

Current sources can be put into two categories depending how the generation of current is managed. In the first type, the generation of the current is controlled by the voltage in point or points of an active component of the source. In the second category, active devices are in power of control of the generation of the current (Seoane et al. 2008). In this work the first category is implemented with an application of a single operational amplifier as a Voltage Controlled Current source (VCCS). The operational amplifier in this design is setup as inverting configuration, i.e. it inverts or shifts the output by 180°.

3.2.1 Voltage Controlled Current source (VCCS)

3.2.1.1 *Load-in-the-Loop*
Load-in-the-Loop is a VCCS with a single operational amplifier as an active component of the system. The biological tissue, the load, is put in the negative feedback path of the operational amplifier. This type of load is called a floating load, i.e. the load is not grounded directly to the system's ground.

The requirement mentioned above for the current sources, i.e. high output impedance, is satisfied from the property of the operational amplifier implemented. The ideal characteristics of an operational amplifier present infinite input impedance and its frequency dependency to this setup of current source (Storr 2012).
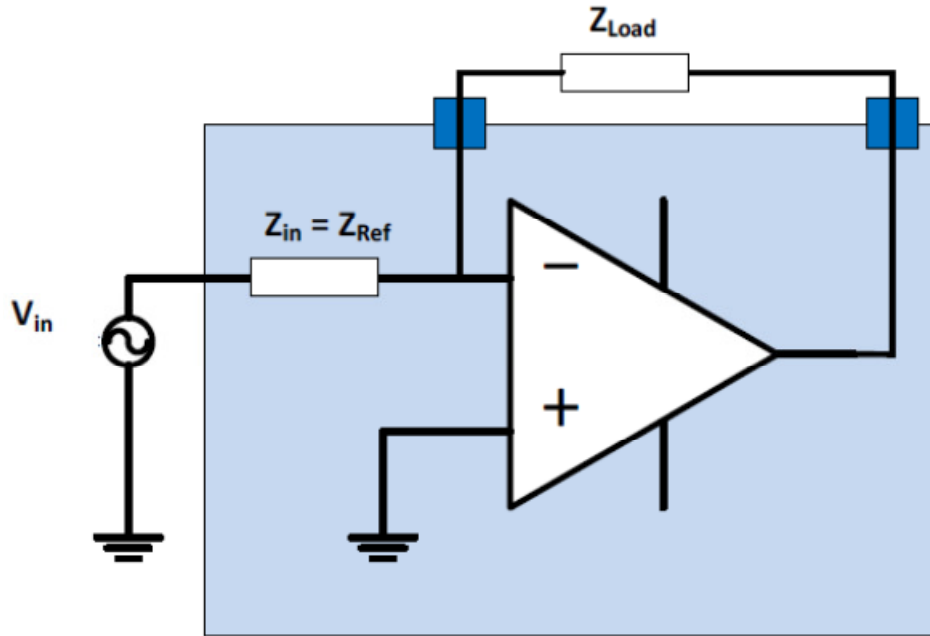
Figure 3-2 Load-in-the-Loop Single Operational Amplifier Voltage Controlled Current Source.

When coming to practical work the output impedance is finite and also it decreases as a function of frequency. This infinite output impedance of the current source allows generating the stimulating current without the interference of the impedance of the biological tissue Z_{Load} in the diagram (Seoane 2007).

3.2.1.2 *Practical Load-in-the-loop VCCS Design*

When designing the current source patient safety has to be taken in to consideration and it has to follow the IEC 60601 guideline. The limit of the injected current is dependent on its frequency. As frequency increase, the value of the stimulating current as well increases.
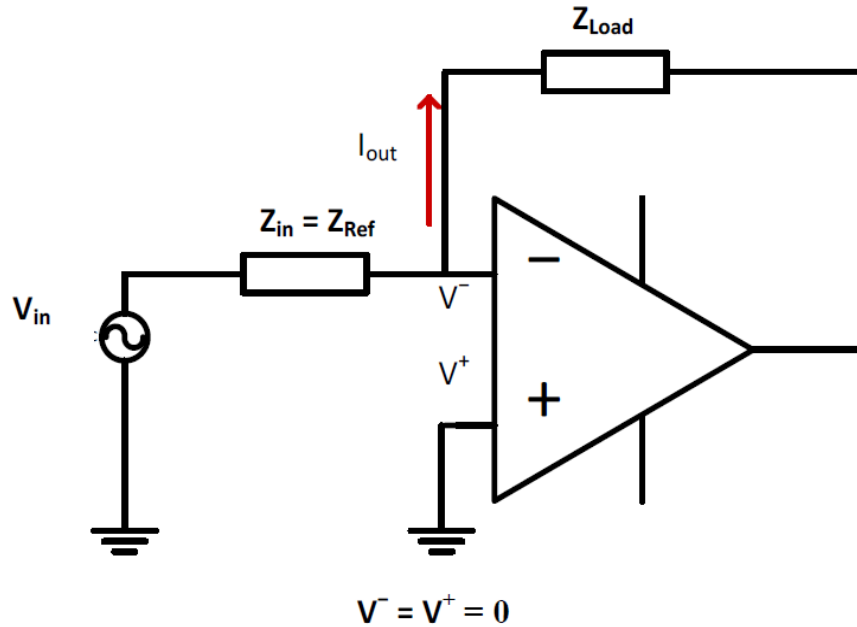
Figure 3-3 Practical Single Operational Amplifier Voltage Controlled Current Source Design.

Adjusting Z_{in} to the required value can give a freedom to control the injection current, hence the name voltage controlled current source.

3.3   Data Acquisition and Analysis Hardware

3.3.1   National Instruments NI USB-6218

The NI USB-6218 is a plug-and-play USB connected data acquisition device. It is powered from its USB bus. In this work the National Instruments NI USB-6218 is used as a multipurpose hardware for:-. AC signal generation at the required frequency and amplitude to the current source, measuring the response voltage from the test circuit are done using it.

The NI USB-6218 has 32 analog inputs when it is used in a single ended mode. This number is reduced by half when it is applied in a differential mode. The sampling rate is dependent on the number of analog inputs that are used. It is 250kS per second for a one analog input channel and it is divided by the number of analog inputs when there are two or more analog channels are at use. The input voltage range is ± 10 volts

Unlike the analog inputs the sampling rate of the analog outputs is not depend on the number of channels used. It has two analog outputs with each channel update rate of 250kS per second. Output voltage range is ± 10 volts. It has also eight digital inputs and outputs (National Instruments 2011).

Figure 3-4 NI USB-6218.

3.3.2   Merits and Limitations of NI USB-6218

The first advantage of the NI USB-6218 is its bus-powered USB connection. This makes it easily powered by a battery driven computer and in turn make the device safe for application on living tissues. Its handy and compact design is an additional merit that is needed to construct a portable medical device.

Low speed of sampling rate is one of its drawbacks. When coming to analog input sampling, the division of the sampling rate to the corresponding number of analog inputs is another flaw. This drawback makes a restriction in generating high frequency AC signals. The limited number of analog output channel i.e. two, is also additional demerit of the NI USB-6218. This condition limits the number of AC signals used in a multi-frequency application.

3.4   Measurement Systems

Before taking measurement using DAQ devices like the NI USB-6218 types of signal sources and its measurement modes has to be noted. Below are the two types of signal sources and three types of measurement modes are discussed.

3.4.1   Signal Sources

3.4.1.1   *Grounded Signal Sources*

This signal sources are connected to a systems ground. It also shares a common ground point with the device in which the measurement has taken (National Instruments 2003a).
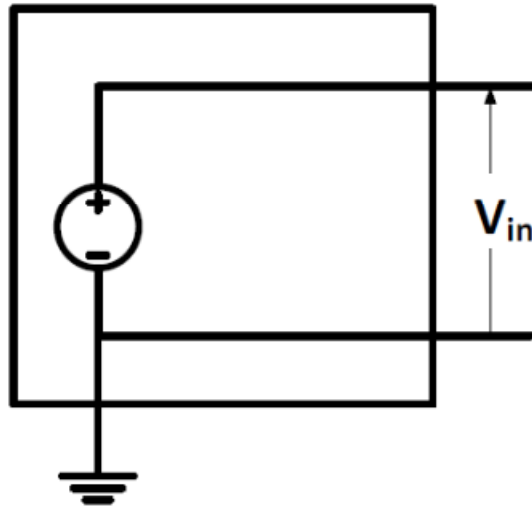
Figure 3-5 Grounded Signal Source.

3.4.1.2 Floating Signal Sources

In this type of signal sources, the voltage signal is not connected to any of common ground. The measurement device's ground point is not also connected to the signal source (National Instruments 2003a).
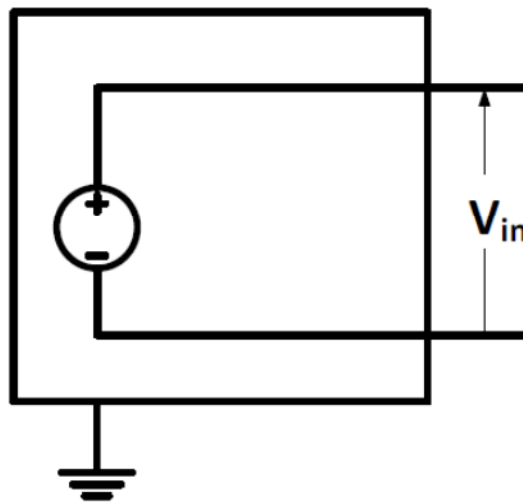
Figure 3-6 Floating Signal Source.

3.4.2 Measurement Systems Modes

3.4.2.1 Differential Mode

Two channels of the measurement system are used for each signal and neither of these is connected to a reference point like earth of the building etc. From its connection layout, it is seen that it rejects common mode voltage (i.e. occurs when the measurement is taken between the input and the reference or earth point and the voltage at the reference or earth point is not zero) and noise (National Instruments 2003a).

17
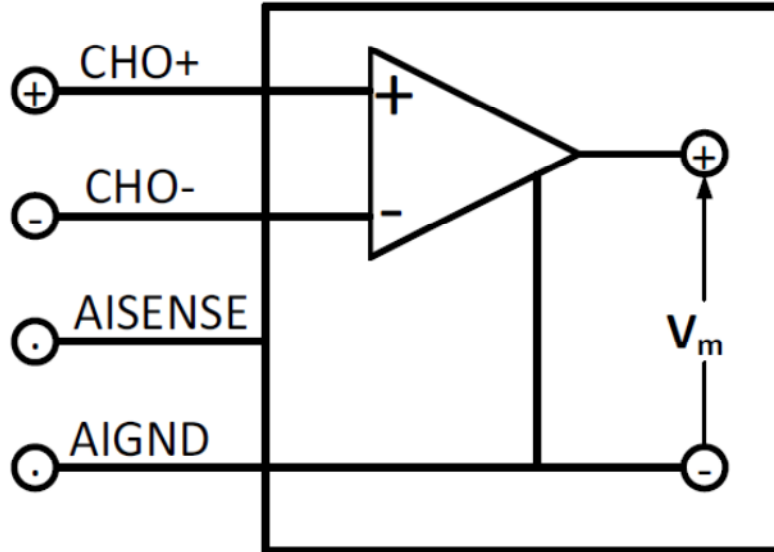
Figure 3-7 Differential Mode Measurement Setup.

3.4.2.2 Referenced Single-Ended Mode (RSE)

The measurement is taken in-between the input and the ground point of the system (AIGND). In this mode one channel is used in measuring each signal. Unlike the differential mode, RSE does not reject the common mode voltage (National Instruments 2003a).
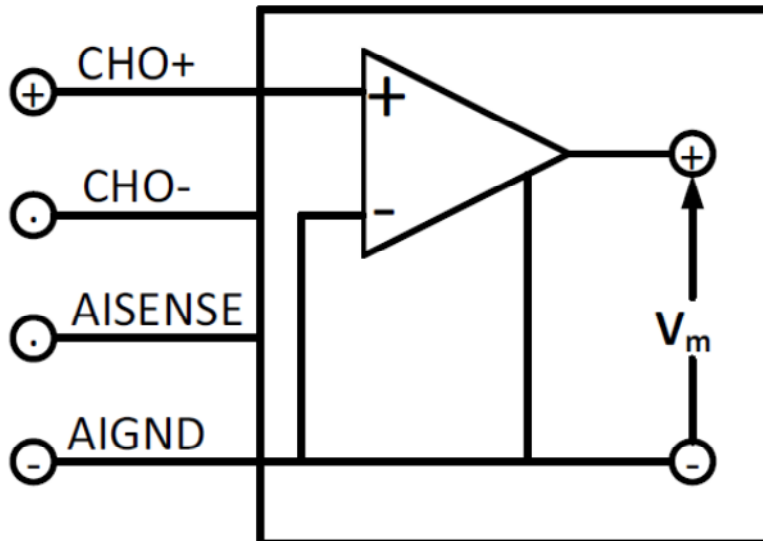
Figure 3-8 Referenced Single-Ended Mode Measurement Setup.

3.4.2.3 Non-Referenced Single-Ended Mode (NRSE)

In this mode measurements are taken with respect to a single analog input which is named AISENSE (National Instruments 2003a).
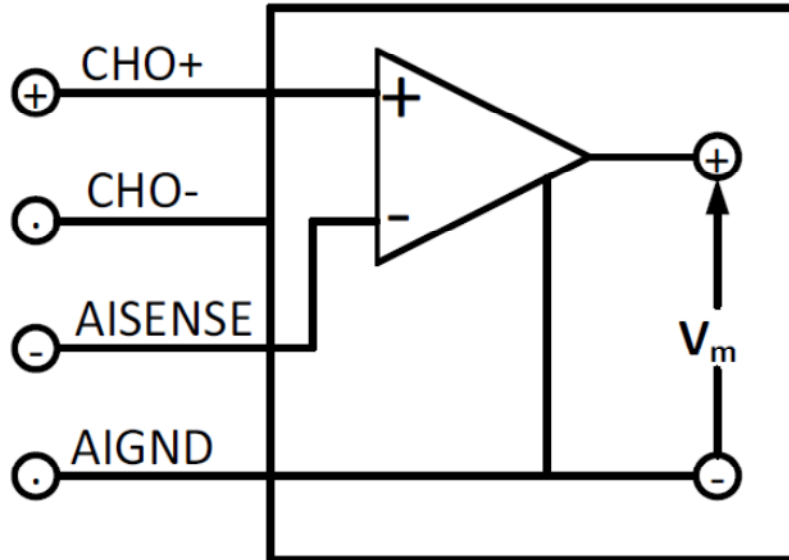
Figure 3-9 Non-Referenced Single-Ended Mode (NRSE) Measurement Setup.

3.5   Laboratory Virtual Instrument Engineering Workbench (LabVIEW™)

This work has been entirely implemented using the National Instruments Laboratory Virtual Instrument Engineering Workbench (LabVIEW). LabVIEW is a graphical programming language. It is implemented using blocks of functions instead of lines of codes that are used in text based programming languages. LabVIEW execution of the program follows the flow of data, hence it is dataflow programming.

The LabVIEW's user interface is called the Front Panel. The functional blocks are put in a separate panel called the Block Diagram. The functional blocks put in Block Diagram controls the Front Panel components (National Instruments 2003b).

3.6   Impedance Estimation Methods

Nowadays impedance measurement systems can be divided in two distinct approaches of measurement methods, depending on the frequency contents of the stimulating signal. Therefore the approaches are basically two: when the stimulation contains several frequencies and when a single frequency is used to perform the measurement.

In multifrequency or multitone measurement signals, the stimulating signal applied to the biological tissue contains two or more signals at different frequencies. If the number of tones is sufficiently large and its distribution is broad enough, to get the impedance spectrum, a single stimulation is enough. When using a single tone measurement; the exciting signal has a single frequency(Seoane et al. 2008).On this approach the impedance spectrum can be obtained by sweeping a single frequency through the range of the measurement.

The measurements taken by the above mentioned approaches are estimated in different manners from the measured values of voltage and AC current (Seoane 2007). Digital Sine Correlation

(DSC), Total Least Square (TLS) and Fast Fourier Transform (FFT) are some of the available estimation methods.

3.6.1 Single Frequency measurement Estimator

3.6.1.1 Digital Sine Correlation (DSC)

In this work Digital Sine Correlation (DSC) is implemented in estimating the impedance at a single frequency measurement system. As biological tissue with impedance value of Z is excited by applying a sinusoidal current $\sin(\omega_m t)$ with a known value of amplitude I .Then the response voltage V_m in the biological tissue is provided by:

$$V_m(t) = I \sin(\omega_m t) \times |Z| \angle \theta$$
$$V_m(t) = I|Z| \sin(\omega_m t + \theta)$$
$$V_m(t) = V_m \sin(\omega_m t + \theta) \quad [v]$$
$$V_m(t) = V_{ip} \sin(\omega_m t) + V_{ip} \cos(\omega_m t)$$

Equation 3.1

Equation 3.1 shows the response voltage is a cumulative of the voltage in phase with the injected current with the voltage drop V_{ip}, it is the voltage across the resistive part of the tissue and the voltage with a 90° phase shift, i.e. in-quadrature, with the injected current with a voltage drop V_{iq}, it is the voltage across the reactive part of the tissue (Seoane 2007).
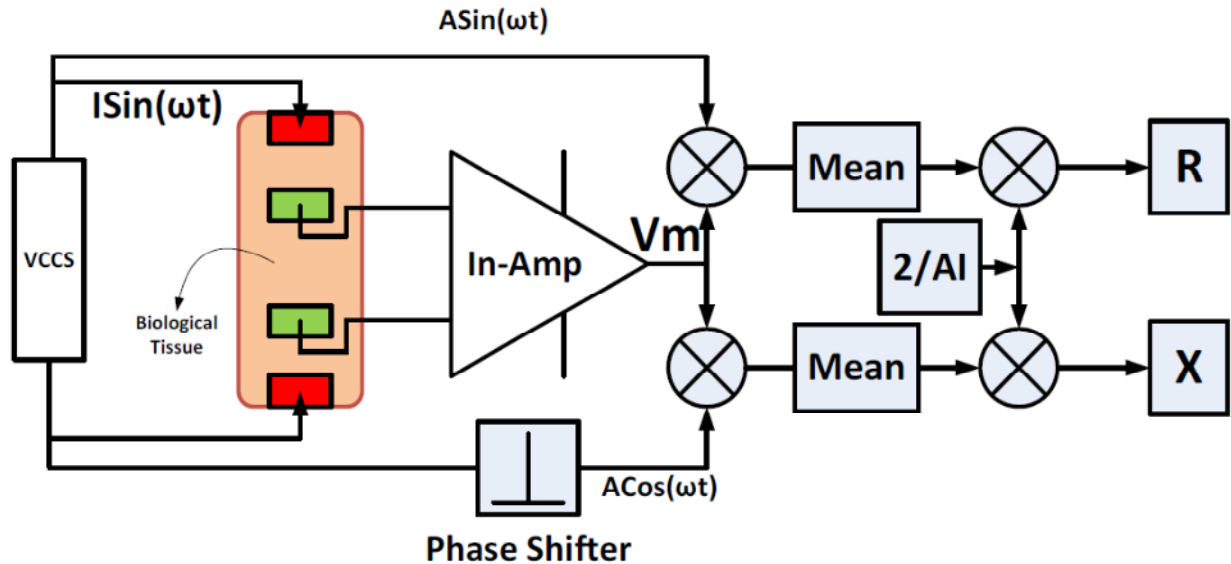
Figure 3-10 Digital Sine Correlation Estimation Method Block Diagram.

From the signal generator of the excitation, two sinusoidal signals one in phase and the other in-quadrature with the injected current and having a unit value of amplitude A is generated as a reference signal. These two signals modulate the two components of Equation 3.1 i.e. the in phase component V_{ip} is modulated by in phase reference signal and the in-quadrature component V_{iq} is modulated by the in-quadrature reference signal. These results $i_p(t)$ and $i_q(t)$ respectively which is shown in the following equations (Seoane 2007).

$$i_p(t) = A\sin(\omega_m t)\, V_m = A\sin(\omega_m t)\,[V_{ip}\sin(\omega_m t) + V_{iq}\cos(\omega_m t)]$$
$$i_p(t) = AV_{ip}\sin^2(\omega_m t) + AV_{iq}\sin(\omega_m t)\cos(\omega_m t)] \qquad [A^2\Omega]$$

Equation 3.2

Here applying double angle trigonometric relationship given below:
$$\cos(2\omega_m t) = 1 - 2\sin^2(\omega_m t) = 2\cos\cos(\omega_m t)^2(\omega_m t) - 1$$

Equation 3.3

$$\sin 2(\omega_m t) = 2\sin(\omega_m t)\cos(\omega_m t)$$

Equation 3.4

Inserting Equation 3.3 and Equation 3.4 to Equation 3.2 gives and i_p(t) is solved as follows

$$i_p(t) = AV_{ip}\left[\frac{1 - \cos(2\omega_m t)}{2}\right] + AV_{iq}\left[\frac{\sin 2(\omega_m t)}{2}\right]$$

$$i_p(t) = \frac{AV_{ip}}{2} - \frac{AV_{ip}\cos(2\omega_m t)}{2} + \frac{AV_{iq}\sin 2(\omega_m t)}{2}$$

$$i_p(t) = \frac{AV_{ip}}{2} + \frac{AV_{iq}}{2}[\sin 2(t) - \cos(2\omega_m t)]$$

Equation 3.5

and i_q(t) is solved from

$$i_q(t) = A\cos(\omega_m t)\, V_m = A\cos(\omega_m t)\,[V_{ip}\sin(\omega_m t) + V_{iq}\cos(\omega_m t)]$$
$$i_q(t) = AV_{ip}\cos(\omega_m t)\sin(\omega_m t) + AV_{iq}\cos^2(\omega_m t)] \qquad [A^2\Omega]$$

Equation 3.6

Inserting Equation 3.2 and Equation 3.3 in Equation 3.6 gives

$$i_q(t) = AV_{ip}\left[\frac{\sin 2(\omega_m t)}{2}\right] + AV_{iq}\left[\frac{1 + \cos(2\omega_m t)}{2}\right]$$

$$i_q(t) = \frac{AV_{iq}}{2} + \frac{AV_{iq}\cos(2\omega_m t)}{2} + \frac{AV_{ip}\sin 2(\omega_m t)}{2}$$

$$i_q(t) = \frac{AV_{iq}}{2} + \frac{AV_{ip}}{2}[\cos(2\omega_m t) + \sin 2(\omega_m t)]$$

Equation 3.7

From Equations 3.5 and 3.7 i_p(t) and i_q(t) are periodic with $i_{p0} = \frac{AV_{ip}}{2}$ and $i_{q0} = \frac{AV_{iq}}{2}$ respectively. It can be deduced that

$$i_{p0} = \int_T i_p(t)dt = \frac{AV_{ip}}{2} \qquad\qquad [A^2\Omega]$$

<div align="right">Equation 3.8</div>

$$i_{q0} = \int_T i_q(t)dt = \frac{AV_{iq}}{2} \qquad\qquad [A^2\Omega]$$

<div align="right">Equation 3.9</div>

Since V_{ip} and V_{iq} are voltage drops across the resistive and reactive part of the tissue and I is the amplitude of the injected voltage. Then the respective resistive part R and reactive part X can be expressed as

$$R = \frac{V_{ip}}{I} = \frac{2i_{p0}/A}{I} = \frac{2}{I}\int_T i_p(t)dt \qquad [\Omega]$$

<div align="right">Equation 3.10</div>

$$X = \frac{V_{iq}}{I} = \frac{2i_{q0}/A}{I} = \frac{2}{I}\int_T i_q(t)dt \qquad [\Omega]$$

<div align="right">Equation 3.11</div>

From Equation 3.10 and 3.11 $Z = R + jX$ can be found (Seoane 2007).The following block diagram depicts the implementation of this method in this work.
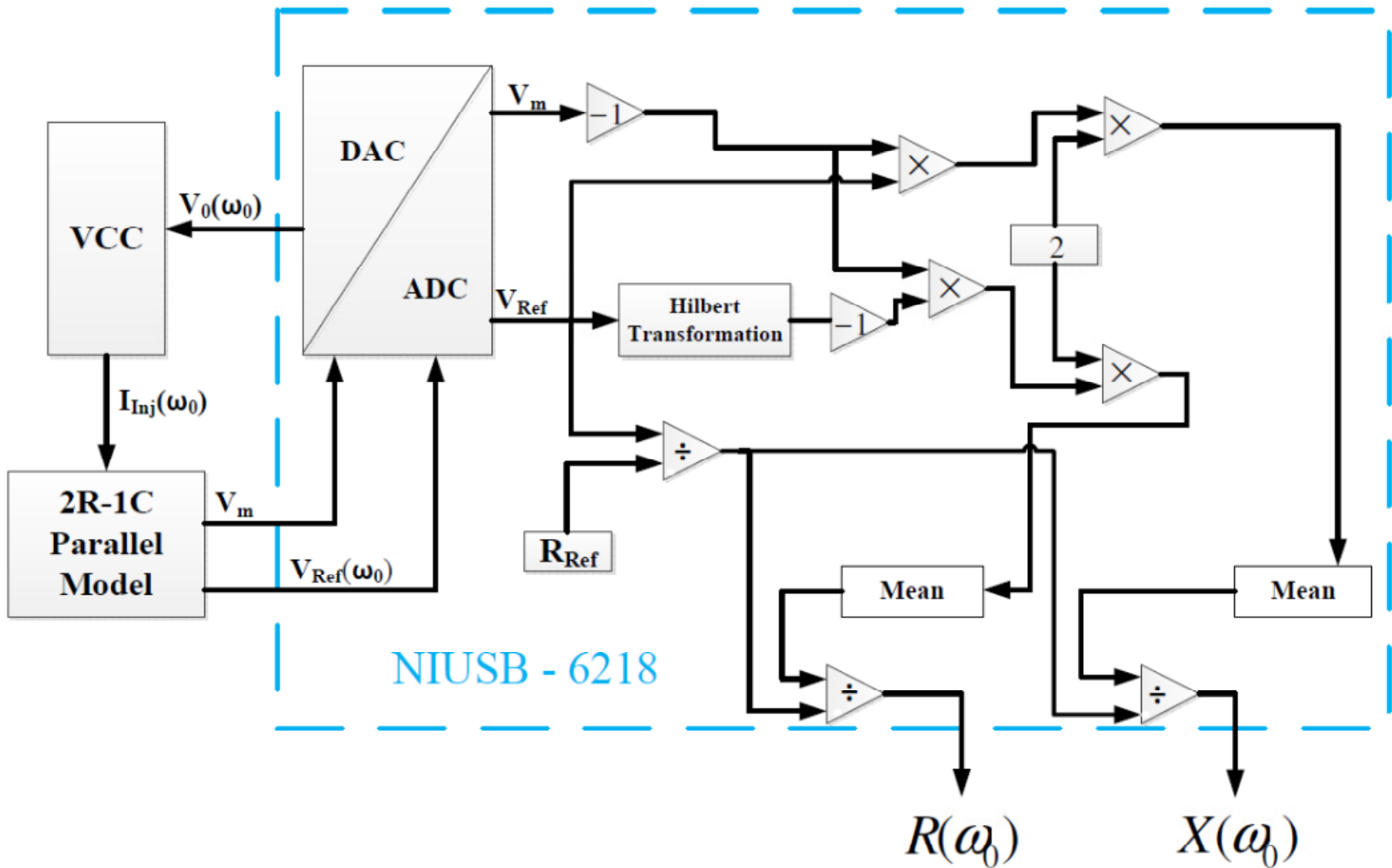
Figure 3-11 Digital Sine Correlation LabVIEW Implementation.

3.6.2　Multifrequency Bioimpedance Measurement Estimators

3.6.2.1　Total Least Square (TLS) Method

The Total Least Square (TLS) is one of bioimpedance measurement estimation methods. In this work the Singular Value Decomposition (SVD) is its computational tool to solve for solutions, i.e.to solve for the resistive and reactive parts of the impedance of the biological material. It is a continual derivation of Least Square (LS) method. Golub and Van Loan introduced it as a way of solving system of equations that are called overdetermined system of equations of the form

$$AX \approx B$$

<div align="right">Equation 3.12</div>

Where $A \in \mathbb{R}^{r \times c}$ and $B \in \mathbb{R}^{r \times d}$ are the know quantities and $X \in \mathbb{R}^{c \times d}$ is the quantity to be determined (I.Markovskya 2007).

The LS approach assumes that only the right side of Equation 3.12 which is B suffers from errors, in this case noise, while the A part at the left side of the equation is free from it. But in practice the error or noise is not restricted only in the right side of the equation. The error showed up in both sides of the equation and this can be analogues to the measurement procedures; there are errors in both sides of the measurement system, in this case in the current injection side and the observation side as well. Here is TLS is useful when the errors are assumed to be occurred in both sides of the equation (S. Van Huffel 1991).

Whenever r > c, i.e. the number of measurements are more than that of the channels in the measurement system, exact solution is not derived for X instead the approximate value of it is looked for (I.Markovskya 2007). Hence, TLS is applied to solve for the estimated values of X when the system under study have disturbances, noises, errors or in general perturbation in both sides, i.e. in both A and B.

Estimation of EBI using the TLS approach requires the in-phase and in-quadrature versions of the injected current to the biological material under study and the observation voltage across the biological material. These quantities can be collected using the same measurement setup as that of Digital Sine Correlation (DSC) method with some modifications which is discussed in section 3.6.1.1 of this work. The modified measurement setup is shown below that is used to get the components of EBI estimation implementing TLS approach.
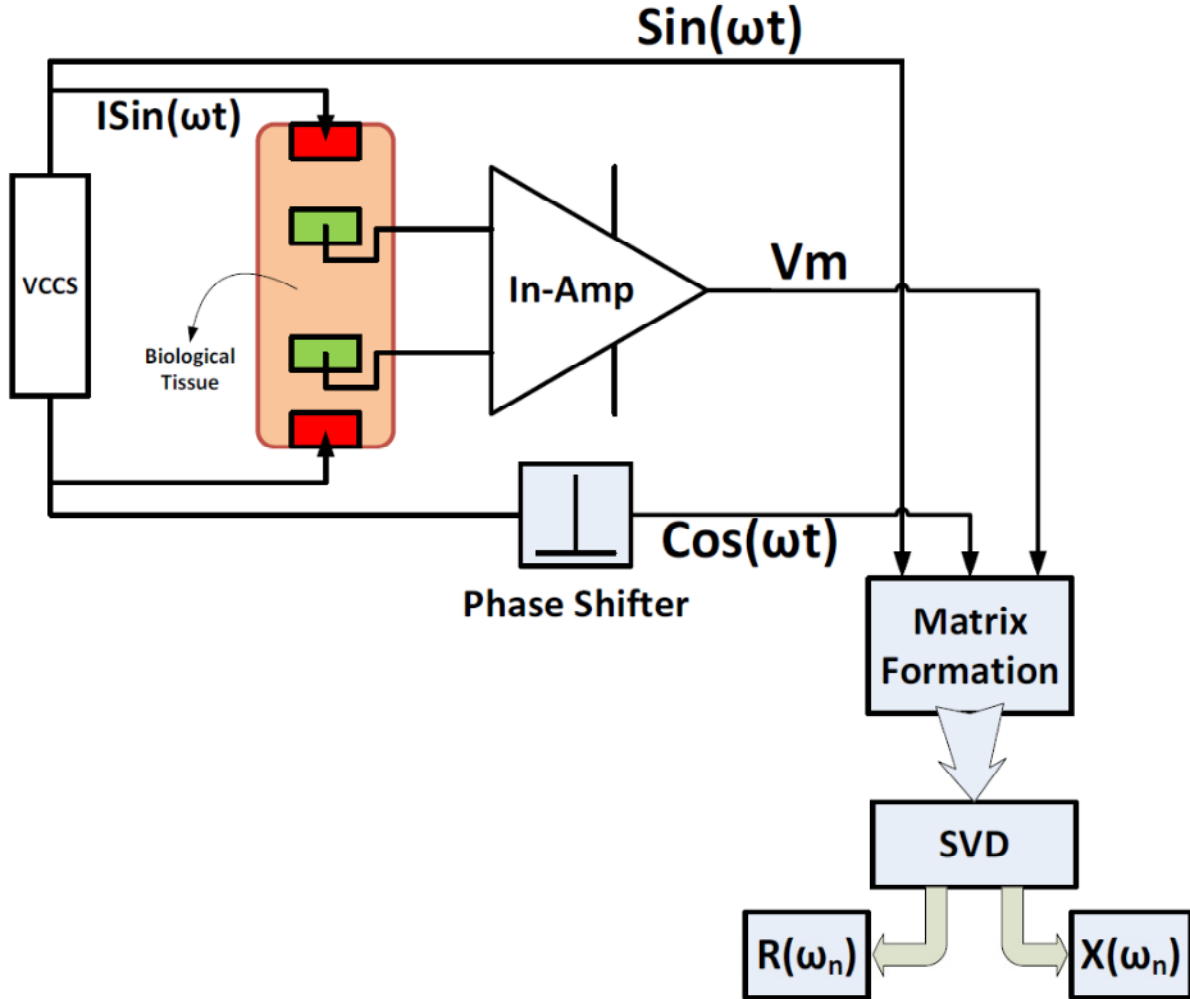
Figure 3-12 Measurement Setup for EBI Estimation Using TLS with In-Phase (Sin (ωt)), In-Quadrature (Cos (ωt)) and Measurement Voltage V$_m$.

It is shown in the figure that all the required quantities for the EBI estimation using TLS are derived and presented. The box labeled VCCS is discussed in detail in the later section of this work for the multifrequency measurement system.

3.6.2.1.1 *Single Frequency Approach*
At first the single frequency approach of the estimation is presented and its generalized multifrequency approach is put afterwards.
To start with the measurement voltage V$_m$ given by

$$V_m(r) = i(r) \times Z(r)$$

Equation 3.13

When frequency $\omega = \omega_m$

$$V_m(r) = I \ \sin(\omega_m r)Z\ (\omega_m)$$

Equation 3.14

Z is a complex quantity at frequency ω_m, and is given by

$$Z(\omega_m) = R(\omega_m) + jX(\omega_m)$$

Equation 3.15

Since V_m is an additive combination of the voltage drops across the resistive and reactive part of the bioimpedance and it can be expressed as

$$V_m(r) = I\sin(\omega_m r) \times R(\omega_m) + I\cos(\omega_m r) \times X(\omega_m)$$

Equation 3.16

As it is mentioned above V_m has two components that have sine and cosine functions. The part that has a sine function which is given as

$$I\sin(\omega_m r) \times R(\omega_m)$$

Equation 3.17

is in-phase with the stimulating or injected current and represents the voltage drop across the resistive part of the biological material. The part that has a cosine component given by

$$I\cos(\omega_m r) \times X(\omega_m)$$

Equation 3.18

is in-quadrature with the injected current and it gives a voltage drop across the reactive part of the biological material.

Using matrix form of representation, the Equation 3.16 can be put in the following way

$$[I\ \sin(\omega_m r) \quad I\ \cos(\omega_m r)] \times \begin{bmatrix} R(\omega_m) \\ X(\omega_m) \end{bmatrix} = [V_m(r)]$$

Equation 3.19

A simplified version of this equation is given by

$$[I]_{r\times 2} \times [Z]_{2\times 1} = [V_m]_{r\times 1}$$

Equation 3.20

The TLS is an approach to solve equations like given in Equation 3.20 as it is discussed when there is a perturbation on both sides of the equation. The perturbations in this case are the noises in the reference current I in the left side and the observation voltage V_m across the biological material in the right side and these noises are given ΔI and ΔV_m respectively.
The estimation of Z depends on the noise levels ΔI and ΔV_m that I and V_m respectively suffer. As these noises become smaller the estimation become close to the true value. Applying the perturbations ΔI and ΔV_m to Equation 3.20 equation

$$(I\ +\ \Delta I)_{r\times 2} \times \hat{Z}_{2\times 1} = (V_m + \Delta V_m)_{r\times 1}$$

Equation 3.21

Where $\hat{Z}$ is represents the estimated bioimpedance value.

Gloub and Van Loan stated in (G.H. Golub 1980) Equation 3.21 can be computed applying the Singular Value Decomposition (SVD) for estimating the value of the $\hat{Z}$ that represent estimated bioimpedance value.

$$\hat{I}_{r\times2} \times \hat{Z}_{2\times1} = \hat{V}_{r\times1}$$

Equation 3.22

Where $\hat{I} = (I + \Delta I)_{r\times2}$ and
$\hat{V} = (V_m + \Delta V_m)_{r\times1}$

and its TLS solution can computed

$$[I|V_m]_{r\times3} \times \begin{bmatrix} \hat{Z} \\ -1 \end{bmatrix}_{3\times1} \approx 0$$

Equation 3.23

Application of the SVD to $[I|V_m]_{r\times3}$ that is shown below when $r > c$, $c = 3$ in this particular case

$$SVD([I|V_m]_{r\times3}) = U \times diag(\sigma_1, \sigma_2, \sigma_3) \times V^T$$

Equation 3.24

Since the closest approximation $[\hat{I}|\hat{V}_m]$ of $[I|V_m]$ that minimizes the perturbation is given by

$$[\hat{I}|\hat{V}_m] = [I|V_m] - [\widehat{\Delta I}|\widehat{\Delta V}_m]$$

Equation 3.25

and its SVD is shown as follows

$$SVD([\hat{I}|\hat{V}_m]) = U \times diag(\sigma_1, \sigma_2, 0) \times V^T$$

Equation 3.26

Then the perturbations $[\widehat{\Delta I}|\widehat{\Delta V}_m]$ obtained as

$$[\widehat{\Delta I}|\widehat{\Delta V}_m] = [I - \hat{I}|V_m - \hat{V}_m] = u_3 \times \sigma_3 \times v_3^T$$

Equation 3.27

Then the approximation set is given as

$$[\hat{I}|\hat{V}_m]v_3 = 0$$

Equation 3.28

its TLS solution is

$$[\hat{I}|\hat{V}_m]_{r\times3} \times \begin{bmatrix} \hat{Z} \\ -1 \end{bmatrix}_{3\times1} \approx 0$$

Equation 3.29

and the estimated solution is given by

$$\begin{bmatrix} \hat{Z} \\ -1 \end{bmatrix} = -\frac{v_3}{v_{3,3}} - \frac{1}{v_{3,3}} [v_{1,3}, v_{2,3}]^T$$

<div align="right">Equation 3.30</div>

Since the estimated impedance $\hat{Z}$ is composed of the estimated resistive part $\hat{R}$ and the estimated reactive part $\hat{X}$ and their estimated values are given from Equation 3.30 below

$$\hat{R} = -\frac{v_{1,3}}{v_{3,3}} \text{ and}$$

$$\hat{X} = -\frac{v_{2,3}}{v_{3,3}}$$

<div align="right">Equation 3.31</div>

This result show that the estimated values of the impedance at single frequency and in the succeeding section its derivation for the multifrequency application of bioimpedance measurement is given.

3.6.2.1.2 Multifrequency Total Least Square Approach

The measurement setup that is given in Figure 3-12 is also used in this multifrequency TLS approach. As stated in the single frequency case the overdetermined system of equations $AX \approx B$ where $A \in \mathbb{R}^{r \times c}$ and $B \in \mathbb{R}^{r \times d}$ are given or known values and $X \in \mathbb{R}^{c \times d}$ is the estimation to be determined.

From the given measurement setup the observation voltage V_m can be given as

$$V_m(r) = i(r) \times Z(r)$$

<div align="right">Equation 3.32</div>

Which can be written as the following at some frequency $\omega = \omega_m$ and with the stimulating or injected sinusoidal current I,

$$V_m(r) = I \sin(\omega_m r) \times Z(\omega_m)$$

<div align="right">Equation 3.33</div>

and the impedance Z is a complex quantity that can be given as at the same frequency $\omega = \omega_m$

$$Z(\omega_m) = R(\omega_m) + jX(\omega_m)$$

<div align="right">Equation 3.34</div>

Since here it is assumed that the injected current is given at several different frequencies, the respective measurement voltages V_m at each time the measurement is taken are given as in the following manner

$$V_{m,0}(t_0) = I_0 \ \sin(\omega_0 t_0) \times R_0(\omega_0) + I_0 \ \cos(\omega_0 t_0) \times X_0 +$$
$$I_1 \ \sin(\omega_1 t_0) \times R_1(\omega_1) + I_1 \ \cos(\omega_1 t_0) \times X_1(\omega_1) + \ ... \ +$$
$$I_{c-1} \ \sin(\omega_{c-1} t_0) \times R_{c-1}(\omega_{c-1}) + I_{c-1} \ \cos(\omega_{c-1} t_0) \times X_{c-1}(\omega_{c-1})$$

$$V_{m,1}(t_1) = I_0 \ \sin(\omega_0 t_1) \times R_1(\omega_0) + I_0 \ \cos(\omega_0 t_1) \times X_0 +$$
$$I_1 \ \sin(\omega_1 t_1) \times R_1(\omega_1) + I_1 \ \cos(\omega_1 t_1) \times X_1(\omega_1) + \ ... \ +$$
$$I_{c-1} \ \sin(\omega_{c-1} t_1) \times R_{c-1}(\omega_{c-1}) + I_{c-1} \ \cos(\omega_{c-1} t_1) \times X_{c-1}(\omega_{c-1})$$
$$...$$
$$...$$
$$V_{m,r-1}(t_{r-1}) = I_0 \ \sin(\omega_0 t_{r-1}) \times R_1(\omega_0) + I_0 \ \cos(\omega_0 t_{r-1}) \times X_0 +$$
$$I_1 \ \sin(\omega_1 t_{r-1}) \times R_1(\omega_1) + I_1 \ \cos(\omega_1 t_{r-1}) \times X_1(\omega_1) + \ ... \ +$$
$$I_{c-1} \ \sin(\omega_{c-1} t_{r-1}) \times R_{c-1}(\omega_{c-1}) + I_{c-1} \ \cos(\omega_{c-1} t_{r-1}) \times X_{c-1}(\omega_{c-1})$$

<div align="right">Equation 3.35</div>

Where $V_{m,0}$,$V_{m,1}$,…, $V_{m,r-1}$ are the measurement voltages taken at different times $t_0,t_1,…,t_{r-1}$ with the injected current at frequencies ω_0, ω_1,…, ω_{c-1} and r and c represents the number of times that the measurement taken and the number of frequencies used in the measurement system respectively.

The components with the sine function in Equation 3.35 at time t_0 that are given as

$$I_0 \ \sin(\omega_0 t_0) \times R_0(\omega_0) + \ I_1 \ \sin(\omega_1 t_0) \times R_1(\omega_1) + \ ... \ + \ I_{c-1} \ \sin(\omega_{c-1} t_0) \times R_{c-1}(\omega_{c-1})$$

<div align="right">Equation 3.36</div>

represents the respective resistive voltage drop across the impedance Z at that particular time and it is in-phase with the injected currents of different frequencies to the biological material.

The remaining part that have cosine functions in Equation 3.35 given as

$$I_0 \ \cos(\omega_0 t_0) \times X_0 + \ I_1 \ \cos(\omega_1 t_0) \times X_1(\omega_1) + \cdots + \ I_{c-1} \ \cos(\omega_{c-1} t_0) \times X_{c-1}(\omega_{c-1})$$

<div align="right">Equation 3.37</div>

represents the respective reactive voltage drop across the impedance Z at that particular time and it is in-quadrature with the injected currents of different frequencies to the biological material.

The next step is putting the expression in Equation 3.35 in a matrix form, since it represents measurements taken r times at c different measurement frequencies and r > c. The matrix format of Equation 3.35 is given as

$$\begin{pmatrix} I_0\,\sin(\omega_0 t_0) & I_1\,\sin(\omega_1 t_0) \cdots I_{c-1}\,\sin(\omega_{c-1}t_0) & I_0\,\cos(\omega_0 t_0) & I_1\,\cos(\omega_1 t_0)\cdots I_{c-1}\,\cos(\omega_{c-1}t_0) \\ I_0\,\sin(\omega_0 t_1) & I_1\,\sin(\omega_1 t_1) \cdots I_{c-1}\,\sin(\omega_{c-1}t_1) & I_0\,\cos(\omega_0 t_1) & I_1\,\cos(\omega_1 t_1)\cdots I_{c-1}\,\cos(\omega_{c-1}t_1) \\ & \vdots & & \\ I_0\,\sin(\omega_0 t_{r-1}) & I_1\,\sin(\omega_1 t_{r-1}) \cdots I_{c-1}\,\sin(\omega_{c-1}t_{r-1}) & I_0\,\cos(\omega_0 t_{r-1}) & I_1\,\cos(\omega_1 t_{r-1})\cdots I_{c-1}\,\cos(\omega_{c-1}t_{r-1}) \end{pmatrix} \times \begin{pmatrix} R_0 \\ R_1 \\ \vdots \\ R_{c-1} \\ X_0 \\ X_1 \\ \vdots \\ X_{c-1} \end{pmatrix} = \begin{pmatrix} V_{m,0} \\ V_{m,1} \\ \vdots \\ V_{m,r-1} \end{pmatrix}$$

Equation 3.38

This matrix form representation can be put in a simpler form as

$$I_{r\times 2c} \times Z_{2c\times 1} = V_{m,r\times 1}$$

Equation 3.39

When there is a small amount of noise in the injected current I and observation V_m, the estimation of Z is closest to the true value. Assuming the perturbations ΔI and ΔV_m found in the injected current I and observation voltage V_m respectively. The expression in Equation 3.39 can be modified to include the noises on either side of it and the estimated impedance $\hat{Z}$ is also given as follows

$$(I + \Delta I)_{r\times 2c} \times \hat{Z}_{2c\times 1} = (V_m + \Delta V_m)_{r\times 1}$$

Equation 3.40

And the respected estimated values given as

$$\hat{I}_{r\times 2c} \times \hat{Z}_{2c\times 1} = \hat{V}_{m,r\times 1}$$

Equation 3.41

Where $\quad \hat{I} = (I + \Delta I)_{r\times 2c}$ and
$\qquad \hat{V}_m = (V_m + \Delta V_m)_{r\times 1}$

Applying Gloub and Van Loan algorithm(G.H. Golub 1980) the TLS solution for Equation 3.41 is computed in the following expression

$$[I|V_m]_{r\times(2c+1)} \times \begin{bmatrix} \hat{Z} \\ -1 \end{bmatrix} = 0$$

Equation 3.42

Computing the Singular Value Decomposition (SVD) Equation 3.42 results

$$SVD\big((I|V_m)\big) = U \times \text{diag}\,(\sigma_1, \sigma_2, \ldots, \sigma_{2c}, \sigma_{2c+1}) \times V^{\mathrm{T}}$$

Equation 3.43

Where $\sigma_1 \geq \sigma_2 \geq \ldots \geq \sigma_{c+1}$.
Since the closest approximation can be obtained in a condition that the deviation is minimized and leads to the expression

$$[\hat{I}|\hat{V}_m] = [I|V_m] - [\widehat{\Delta I}|\widehat{\Delta V}_m] = U \times \text{diag}\,(\sigma_1, \sigma_2, \ldots, \sigma_{2c}, 0) \times V^{\mathrm{T}}$$

Equation 3.44

Then

$$[\widehat{\Delta I}|\widehat{\Delta V_m}] = [I|V_m] - [\hat{I}|\hat{V}_m] = U_{2c+1} \times \sigma_{2c+1} \times V_{2c+1}^T$$

<div align="right">Equation 3.45</div>

After getting Equation 3.45, the TLS solution can be shown as

$$[\hat{I}|\hat{V}_m]_{r\times(2c+1)} \times \begin{bmatrix} \hat{Z} \\ -1 \end{bmatrix}_{(2c+1)\times1} = 0$$

<div align="right">Equation 3.46</div>

and

$$\begin{bmatrix} \hat{Z} \\ -1 \end{bmatrix}_{(2c+1)\times1} = -\frac{1}{v_{2c+1,2c+1}} v_{2c+1} = -\frac{1}{v_{2c+1,2c+1}} [v_{1,2c+1}, v_{2,2c+1}, \dots, v_{2c,2c+1}]$$

<div align="right">Equation 3.47</div>

Since

$$\hat{Z} = \begin{pmatrix} R_0 \\ R_1 \\ \vdots \\ R_{c-1} \\ X_0 \\ X_1 \\ \vdots \\ X_{c-1} \end{pmatrix}$$

<div align="right">Equation 3.48</div>

From Equation 3.47 and Equation 3.48 the estimation of the resistive and the reactive parts of the biological material can be obtained at each particular measurement frequencies. These is shown in the expressions below first the resistive part

$$\hat{R}_0 = -\frac{v_{1,2c+1}}{v_{2c+1,2c+1}} \quad, \quad \hat{R}_1 = -\frac{v_{2,2c+1}}{v_{2c+1,2c+1}} \quad, \dots, \quad \hat{R}_{c-1} = -\frac{v_{c,2c+1}}{v_{2c+1,2c+1}}$$

<div align="right">Equation 3.49</div>

Where R_0, R1 ,…, Rc-1 are the estimated resistive values at the first, second ,…, and the cth measurement frequencies where c is the number of measurement frequencies used.
and the reactive part is given as

$$\hat{X}_0 = -\frac{v_{c+1,2c+1}}{v_{2c+1,2c+1}} \quad, \quad \hat{X}_1 = -\frac{v_{c+2,2c+1}}{v_{2c+1,2c+1}} \quad, \dots, \quad \hat{X}_{c-1} = -\frac{v_{2c,2c+1}}{v_{2c+1,2c+1}}$$

<div align="right">Equation 3.50</div>

Where X_0, X_1 ,…, X_{c-1} are the estimated reactance values at the first, second ,…, and the cth measurement frequencies where c is the number of measurement frequencies used.

From equations Equation 3.49 and Equation 3.50 the estimated values of the impedance, the resistive part and the reactive part can be obtained using the TLS by implementing the SVD as a computational tool.

Below is the flow chart that is showing the implementation of the TLS in this work to measure the resistive and reactive part of the bioimpedance that is represented by a 2R1C equivalent circuit.
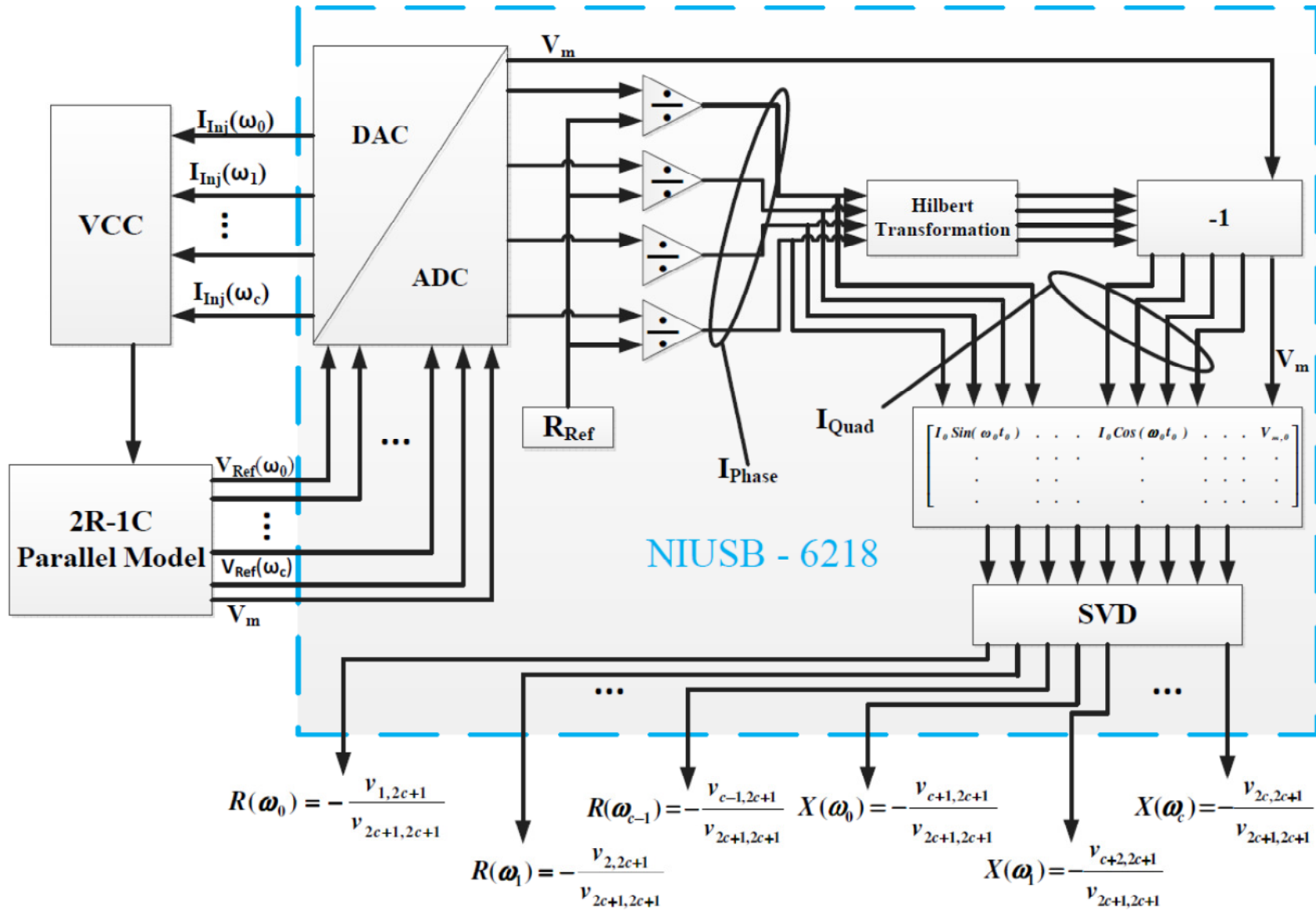
Figure 3-13 Multifrequency EBI Measurement System Implementation –Total Least Square Method.

The implementation is consists of the two NI USB-6218 DAQs, Voltage Controlled Current Source (VCCS) and 2R1C parallel circuit.

3.6.2.1.2.1 NI USB-6218 DAQ

This device is used to generate the voltage to the VCCS and measure all the reference and the response measurement voltage across the 2R1C parallel equivalent circuit. Its detail is discussed in section 3.3 of this work. The basic reason to use two DAQs is the constraints on number of its output channels. Each DAQ has two output channels but in this work four of them is needed and the use of two DAQs comes to fulfill the required number of output channels. From these four channels, four voltages at different frequencies are generated to make them as input for the VCCS to inject a multifrequency excitation current to the 2R1C parallel equivalent circuit.

3.6.2.1.2.2 Multifrequency Voltage Controlled Current Source (VCCS)

The VCCS used for the multifrequency approach is basically the same as that of the single frequency; it is a Load-in-the-Loop configuration that is discussed in detail in section 3.2.1 of this work. The only different thing used here is the use of multiple inputs for the implementation of multiple input voltages that are used to create multiple frequency current injection to the 2R1C parallel equivalent circuit.

The VCCS implemented is a simple inverting Summing amplifier. The numbers of the multiple inputs are decided based on the number of the measurement frequencies that the system intend to have, in this case four then four input branches are used. The following figure shows a simple implementation of an inverting summing amplifier as VCCS that is used in this work.
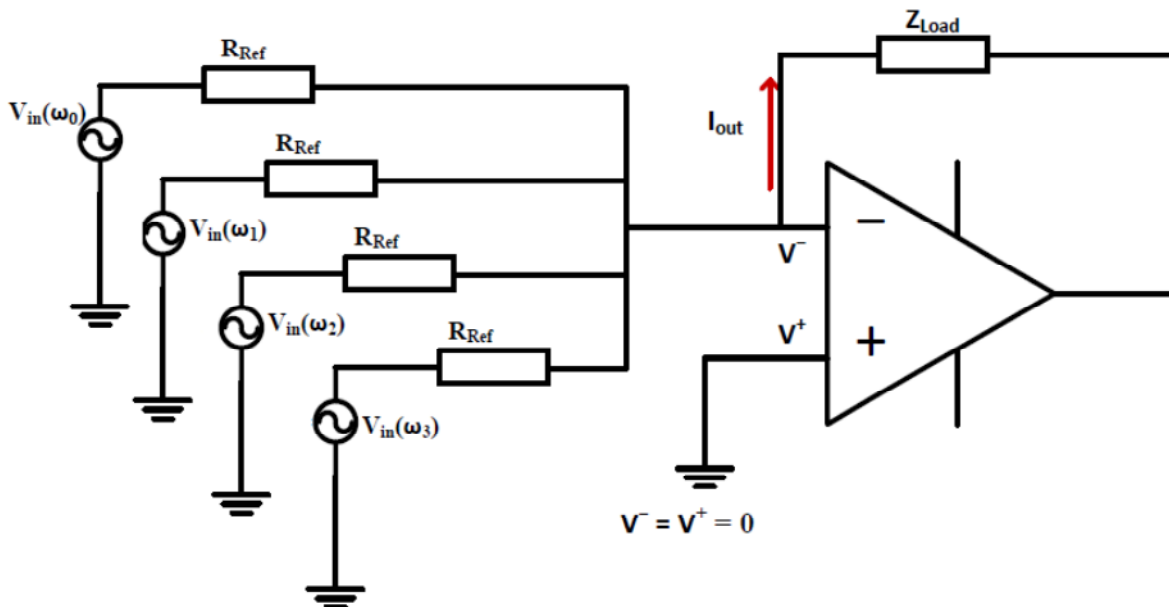
Figure 3-14 Multifrequency EBI Measurement System VCCS.

3.6.2.2 *Synchronization of the DAQs*

The need for generation of multifrequency current injection leads to the use of two NI USB-6218 DAQs. The main reason for the application of the two DAQs is due to their limited number of analog output channels, i.e. each DAQ has two analog output channels. In this work four different measurement frequencies are used, hence two DAQs are used. The individual timers that each DAQ have result in asynchronous reference voltages and measurement voltage that give rise to erratic estimations on the reactive part of the impedance. These errors can easily be shown in the phases of each of the reference voltages and measurement voltage. The phases of the voltages show a significantly large variation instead of reasonably insignificant low variations that can be resulted from the inaccuracies that occur in the measurement setup. These discrepancies of phase that occur due to the asynchronous timers of the individual DAQs shown in the following screen shoot of the system.
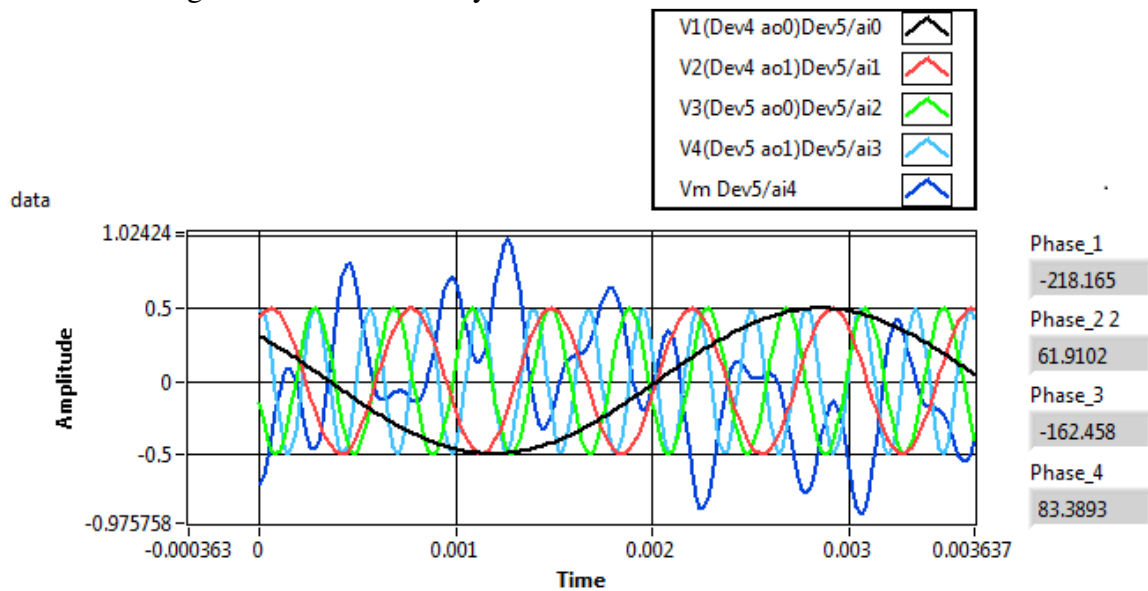
Figure 3-15 Plot showing the four reference voltages at frequencies 300, 1400, 2500 and 3600 Hz and the measurement voltage before synchronization with their corresponding phase shifts at the right side of the plot.

At the origin of the plot the waveforms start at different points which is the result of their phase differences that is shown in the right side of the plot in degrees. From here it is obvious that synchronization of the two DAQs is a first thing to do before acqusation of the referance voltages and measurement voltage.

The synchronization of the devices is achieved by routing out the timing signals, i.e. analog output sample clock and start trigger, of one of the devices to the other using the Programmable Function Interface (PFI) channels that are connected with an external cable inbetween the devices. The PFI signals can individually be configured as a timing input/output signal for analog input and analog output respectivelly (National Instruments 2007).The result of this synchronization is displyed in the plot below.
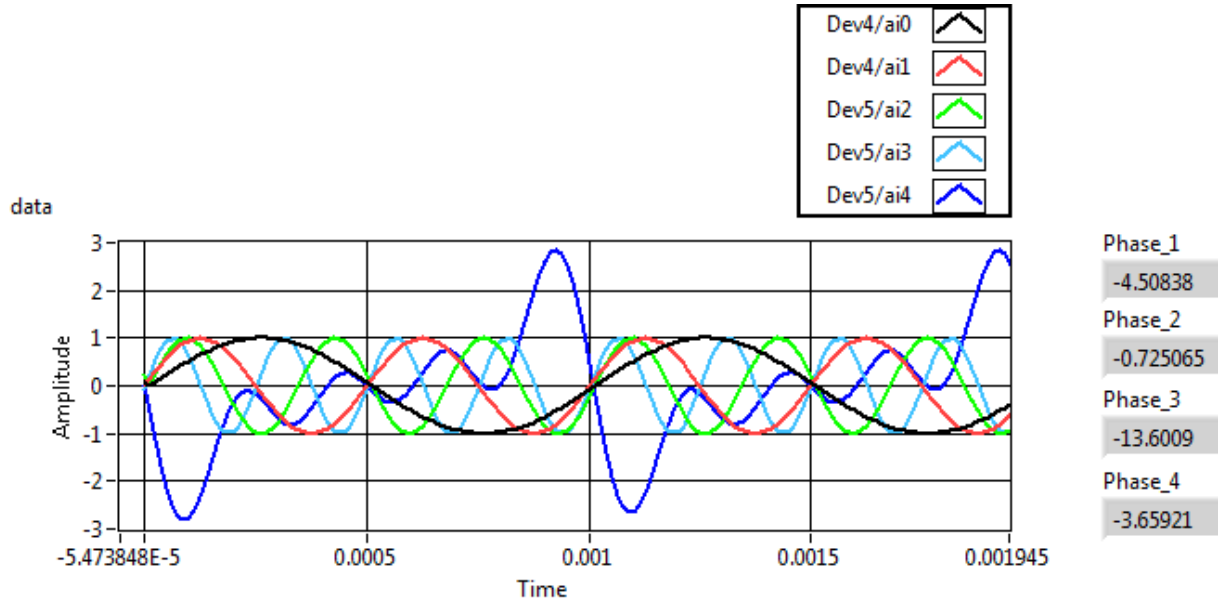
Figure 3-16 Plot showing the four reference voltages at frequencies 1000, 2000, 3000 and 4000 Hz and the measurement voltage after synchronization with their corresponding phase shift at the right side of the plot.

It shows a remarkable improvement on the phase differences of the reference voltages and measurement voltage and their phase is not varying erratically as the program executed everytime. This is helpful in synthesizing and analyzing the signals after the measurement takesplace.

At this level of synchronization also ,some of the reference voltages show a larger phase shift compared to the others and it gives an estimation errors on the reactive component of the impedance again, i.e.it gives positive reactive value, at those particular measurement frequencies. As it is discussed above these phase shifts gives an error in the reactive part. Another approach is also implemented to remove the time delay that is occurred due to these phase shifts. The time delay that is occurred due to the phase shifts is given by the following expression

$$Time\ Shift = \frac{\phi^{\circ}}{360 \times f}$$

Equation 3.51

Where ϕ° is the phase shift in degrees and f is the measurement frequency (Sengpiel).

Finding and removing the time shift also has a limitation whenever the time delay is small compared to the time between each samples i.e. sampling time. At the first and third measurement frequencies this approach is successful since the time shift is almost equal to the time difference between two samples or sampling time. But for the remaining measurement frequencies it is not working due to their small time shift that result estimation errors i.e. the time delay is smaller than the sampling time. The other problem this approach cannot overcome is the phase shift at the measurement voltage. Since the measurement voltage is constructed with the original waveforms not the time shifted signals, this gives an error in the estimation process.

36

The last attainable phase shifts are shown with their corresponding waveforms in the following plot.
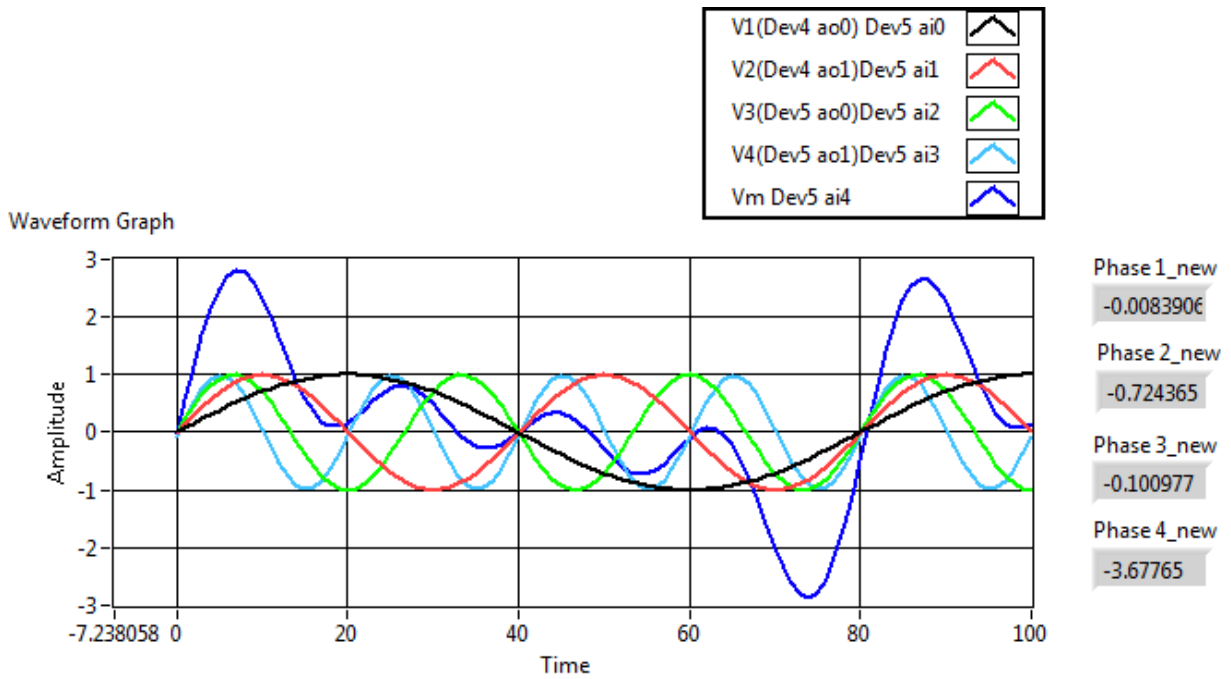
Figure 3-17 Plot showing the four reference voltages at frequencies 1000, 2000, 3000 and 4000 Hz and the measurement voltage after synchronization and time delay removal at the first and third measurement frequency with their corresponding phase shift at the right.

Chapter 4. **Results**

4.1 Measurement Results

The measurement results that are carried out during this work are presented in this chapter. The first section contains the results from the single frequency impedance measurement set up and later to that the results from the multifrequency impedance measurement system setup are presented. As explained before, the single frequency impedance measurement setup is implemented using DSC and the multifrequency impedance measurement setup uses Total Least Squares.

4.2 Single Frequency Measurement

4.2.1 Single Frequency Measurement System GUI

To perform the spectroscopy measurement sweeping using a single frequency a GUI, with controls and displays is build using LabVIEW. The controls are used to vary different parameters of the measurement system like measurement frequency and amplitude sampling frequency, number of periods etc. The waveform of voltages that are measured displayed using waveform charts. The screenshot of the GUI is shown in the following figure below.
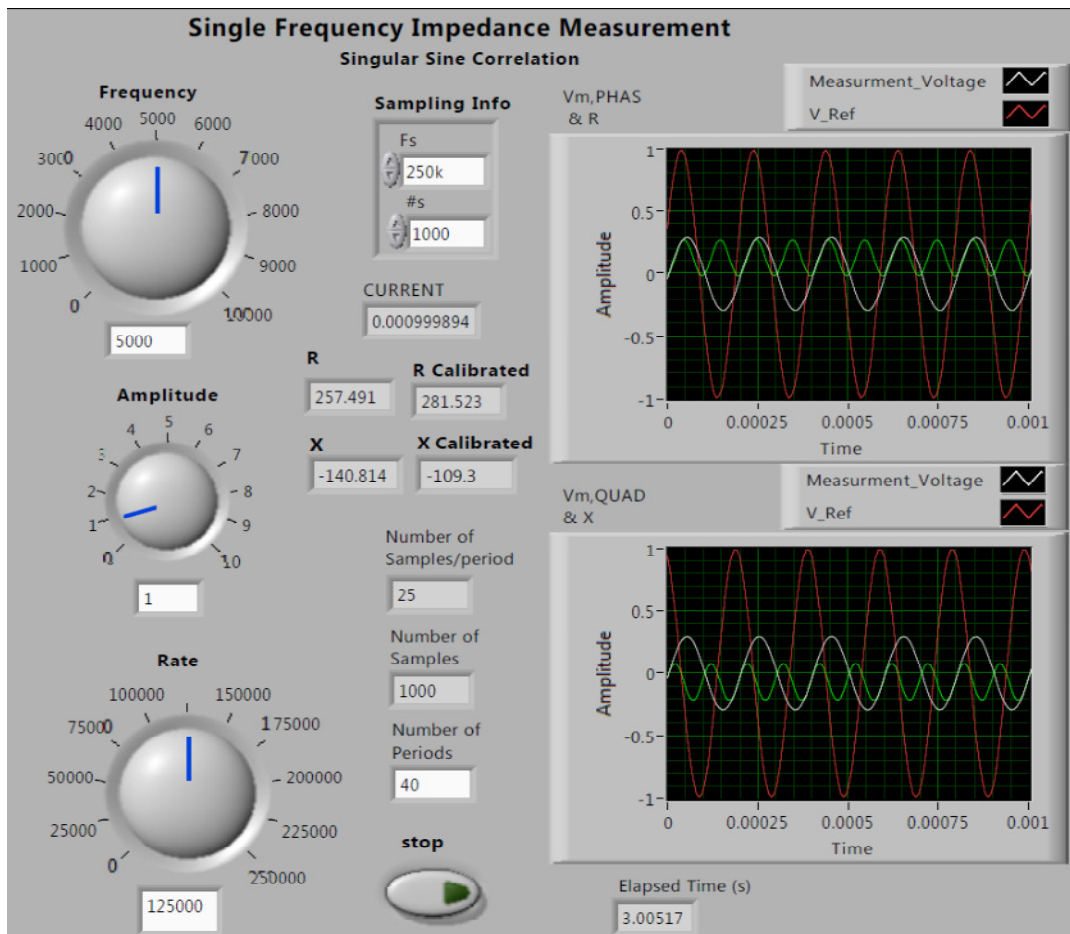
4.2.2 Single Frequency Measurement Results

The result presented at this section are impedance values from the measurements that are taken across the 2R1C equivalent electrical circuit as a load in the set up which is shown in the Figure 3.3. The impedance estimation method used is the single sine correlation method for the single frequency measurement implementation. The schematic connection is shown below.
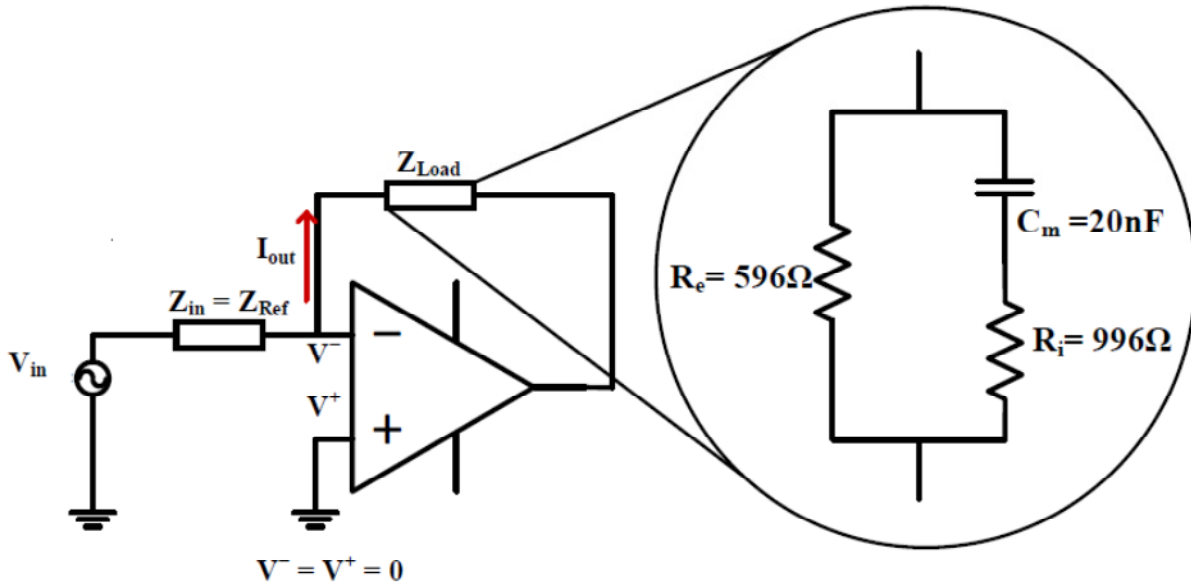
Figure 4-2 Schematic Showing the measurement Setup with the (inset) 2R1C Equivalent Electrical Circuit with Components.

The theoretical values are derived from those particular component values of the 2R1C shown in the Figure 4-2 by calculating the equivalent impedance of it which is given by the following formula which is derived in section 2.3 of this work.

$$Z = \frac{R_e(1 + jR_iC\omega)}{1 + jC\omega(R_i + R_e)}$$

Equation 4.1

The respective R and X values are computed at each measurement frequency from Equation 4.1 by taking the real and imaginary part of the complex Z value.

The calibration of the system performed using one 2R1C parallel circuit with 30nF capacitor in series with 745.4 Ω resistor and in parallel with a 313.7 Ω resistor. Calibration of the estimated measurements done against the theoretical values and a factor developed to improve the estimation. The factor is given as a function of frequency in the following equation:

$$Calibration\ Factor(f) = \frac{Theoretical\ Value(f)}{Measured\ Value(f)}$$

<div align="right">Equation 4.2</div>

Then to get the calibrated value for the measurements

$$Calibrated\ Value(f) = \ Calibration\ Factor(f) \times New\ Measurement\ Value(f)$$

<div align="right">Equation 4.3</div>

The measurements are taken using two different sets of 2R1C circuits. The first set is a 20nF capacitor in series with 996 Ω resistor and in parallel with a 596 Ω resistor and the second 2R1C set is 40nF capacitor in series with 498.5 Ω resistor and in parallel with a 298 Ω resistor.

The measurements, calibrated and theoretical values from Equation 4.1, the two set of measurements of 2R1C circuits are given in the following tables below. Table 4-1 gives the resistive part of the measurement for the 2R1C circuit with 20nF.

Table 4-1 Single Frequency-Resistive Part Estimated, Theoretical and Calibrated values of 20nF 2R1C Circuit.

Measurement Frequency (Hz)	R (Ω) Estimated	R (Ω) Theoretical	R (Ω) Calibrated
100	597.337	595.9107349	596.988
200	596.889	595.6433678	596.54
400	596.423	594.5802787	596.074
600	593.598	592.8308333	594.089
800	590.331	590.4274864	590.82
1000	587.508	587.4135724	587.995
2000	561.484	565.2090284	565.023
3000	526.43	536.9127447	535.752
4000	492.508	508.8965249	507.611
5000	464.378	484.4056069	478.618
6000	438.867	464.2887508	460.067
7000	418.725	448.2263969	445.975
8000	401.916	435.5245981	428.072
9000	385.938	425.4755789	420.647
10000	373.857	417.4792903	407.479
20000	288.734	385.9924173	377.648
30000	212.365	378.9014734	369.103
40000	133.059	376.3051609	363.89
50000	50.6752	375.0822986	355.105

The reactive part of the measurements, calibrated and theoretical values, for the 2R1C parallel circuit with 20nF are given in the following table.

Table 4-2 Single Frequency-Reactive Part Estimated, Theoretical and Calibrated values of 20nF 2R1C Circuit.

Measurement Frequency (Hz)	X (Ω) Estimated	X (Ω) Theoretical	X (Ω) Calibrated
100	-6.02773	-4.461990097	-4.14061
200	-12.0697	-8.91328248	-8.291
400	-24.3575	-17.74149376	-16.7318
600	-36.0335	-26.40224776	-24.6797
800	-47.6947	-34.81835265	-32.6665
1000	-57.7785	-42.91998735	-39.5731
2000	-106.807	-76.95564268	-71.5871
3000	-140.354	-98.45088734	-90.6521
4000	-160.659	-108.8485288	-95.3402
5000	-174.528	-111.5628096	-103.571
6000	-180.564	-109.7283101	-96.5712
7000	-185.274	-105.5227001	-87.9756
8000	-187.992	-100.26874	-89.266
9000	-189.628	-94.7089773	-76.0091
10000	-192.241	-89.23509231	-77.0563
20000	-223.899	-39.3407	-52.48703656
30000	-258.362	-26.1699	-36.17284719
40000	-286.317	-19.5106	-27.45408261
50000	-268.367	-15.5869	-22.08551771

The pictorial representation of the results given in the Tables 4-1 and 4-2 are given in the following two spectral and impedance plot.
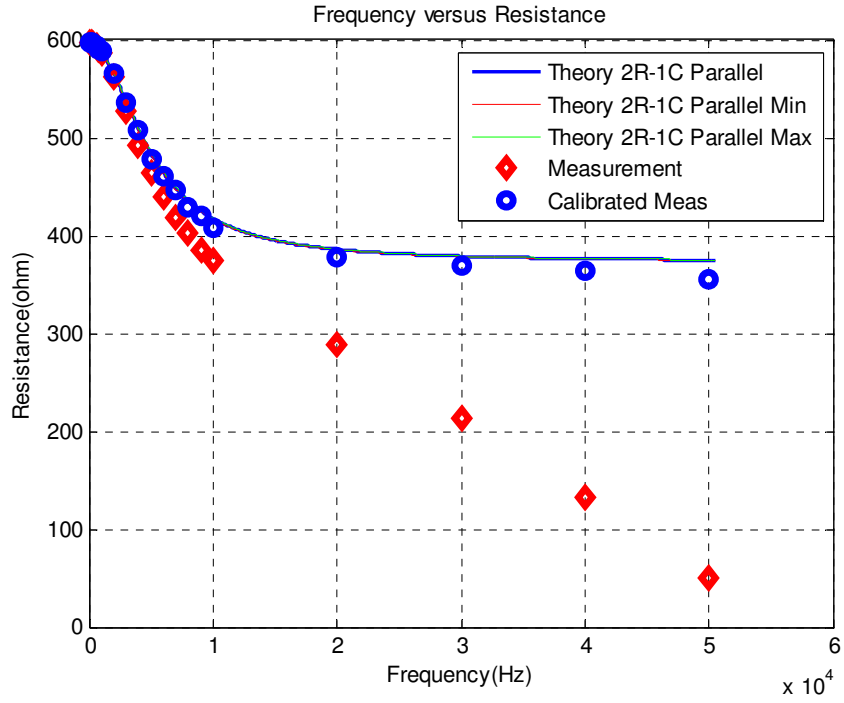
Figure 4-3 Single Frequency-Plot of Frequency versus Resistance Measurement, Theoretical and Calibrated values of 20nF 2R1C parallel model.
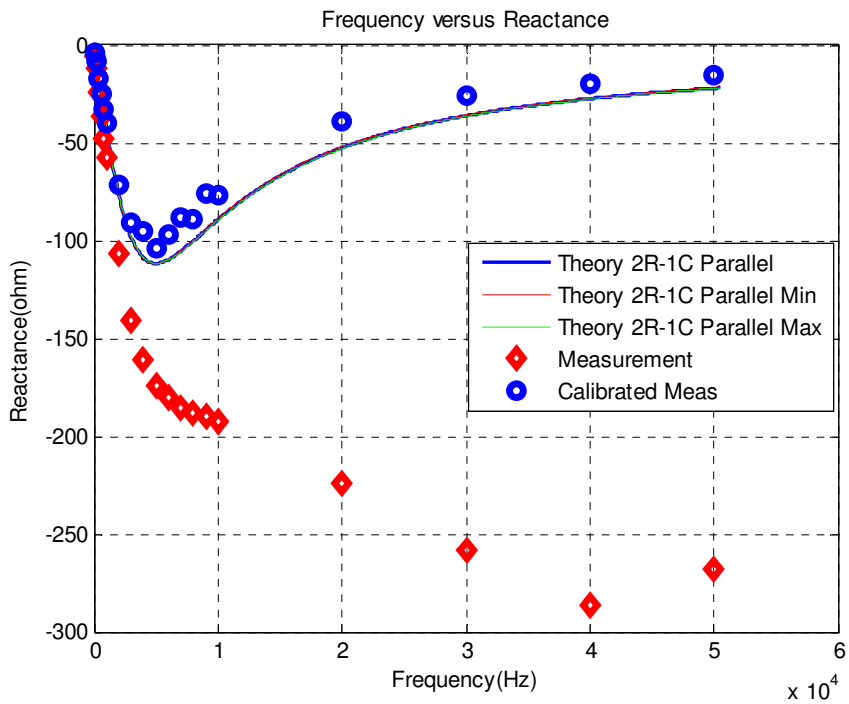
Figure 4-4 Single Frequency-Plot of Frequency versus Reactance Measurement, Theoretical and Calibrated values of 20nF 2R1C parallel model.
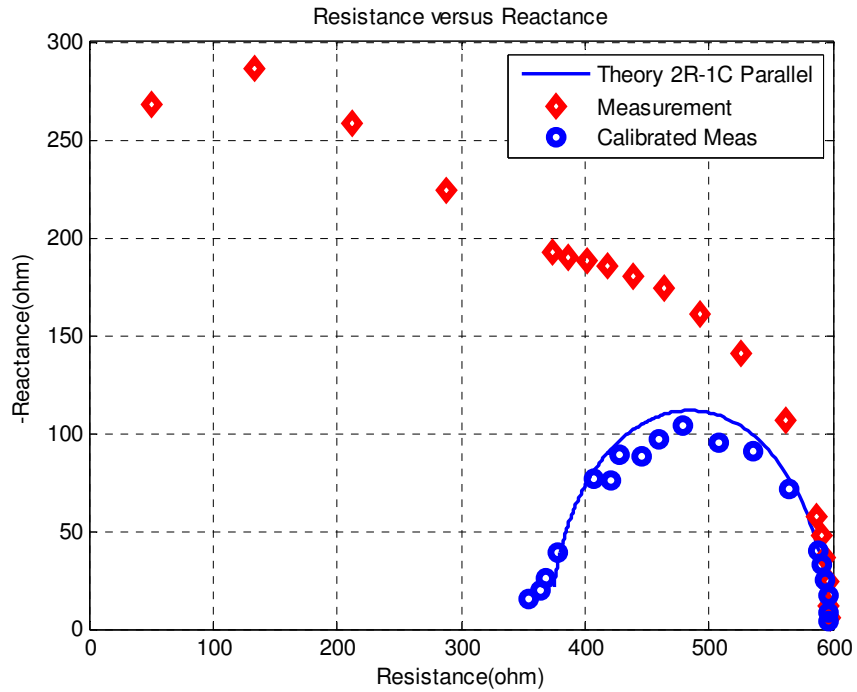
Figure 4-5 Single Frequency-Plot of Resistance versus Reactance Measurement, Theoretical and Calibrated values of 20nF 2R1C parallel model.

The second measurement is taken using a 40nF for the capacitor in the 2R1C parallel circuit. The following tables show the values obtained from the measurement, theoretical and calibrated results for the resistive and reactive part of the impedance.

Table 4-3 Single Frequency-Resistive Part values, Theoretical and Calibrated, for 2R1C Circuit with 40nF.

Measurement Frequency (Hz)	R (Ω) Estimated	R (Ω) Theoretical	R (Ω) Calibrated
100	298.612	297.9553395	298.437
200	298.402	297.8215722	298.227
400	298.209	297.2896991	298.035
600	296.726	296.4144496	296.972
800	295.114	295.2120806	295.359
1000	293.758	293.7042972	294.001
2000	280.542	282.5975148	282.31
3000	263.241	268.4476495	267.903
4000	246.08	254.4422743	253.626
5000	232.975	242.2028244	240.119
6000	219.374	232.1518561	229.971
7000	209.211	224.1282693	222.827
8000	200.992	217.784399	214.072
9000	192.457	212.766093	209.765
10000	186.44	208.7732905	203.208
20000	144.325	193.0543804	188.769
30000	104.97	189.5152002	182.444
40000	65.0211	188.2194182	177.82
50000	23.5723	187.6091184	165.183

The table below gives the reactive values for the part of the measurement, both calibrated and theoretical, from measurements on the 2R1C parallel circuit with 40nF.

Table 4-4 Single Frequency- Reactive Part values, Theoretical and Calibrated for 2R1C Circuit with 40nF.

Measurement Frequency (Hz)	X (Ω) Estimated	X (Ω) Theoretical	X (Ω) Calibrated
100	-3.05319	-2.230993927	-2.09731
200	-6.10805	-4.456632289	-4.19578
400	-12.2795	-8.870675948	-8.43508
600	-17.961	-13.20088826	-12.3017
800	-24.0683	-17.40862995	-16.4846
1000	-29.5488	-21.45895592	-20.2383
2000	-53.5885	-38.4711497	-35.9174
3000	-70.2842	-49.20906748	-45.3953
4000	-80.1762	-54.39757807	-47.5793
5000	-86.6348	-55.74636733	-51.412
6000	-90.2261	-54.82348608	-48.2556
7000	-92.5229	-52.71747423	-43.9336
8000	-93.7881	-50.08909845	-44.5343
9000	-94.8021	-47.30905217	-37.9997
10000	-95.6279	-44.5727303	-38.3307
20000	-112.577	-26.21251429	-19.7805
30000	-130.413	-18.06433578	-13.2097
40000	-144.566	-13.7100771	-9.85118
50000	-135.133	-11.02903608	-7.84863

The pictorial representation of the results given in the Tables 4-3 and 4-4 are given below. The plots are presented in spectral plots and an impedance plot i.e. resistance against reactance.
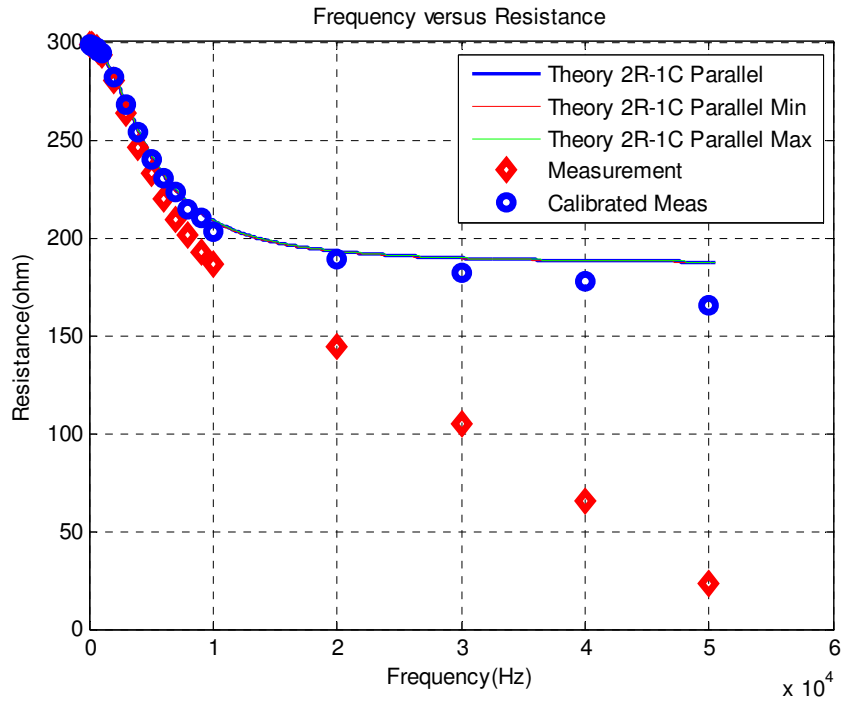
Figure 4-6 Single Frequency-Plot of Frequency versus Resistance Measurement, Theoretical and Calibrated values of 40nF 2R1C parallel model.
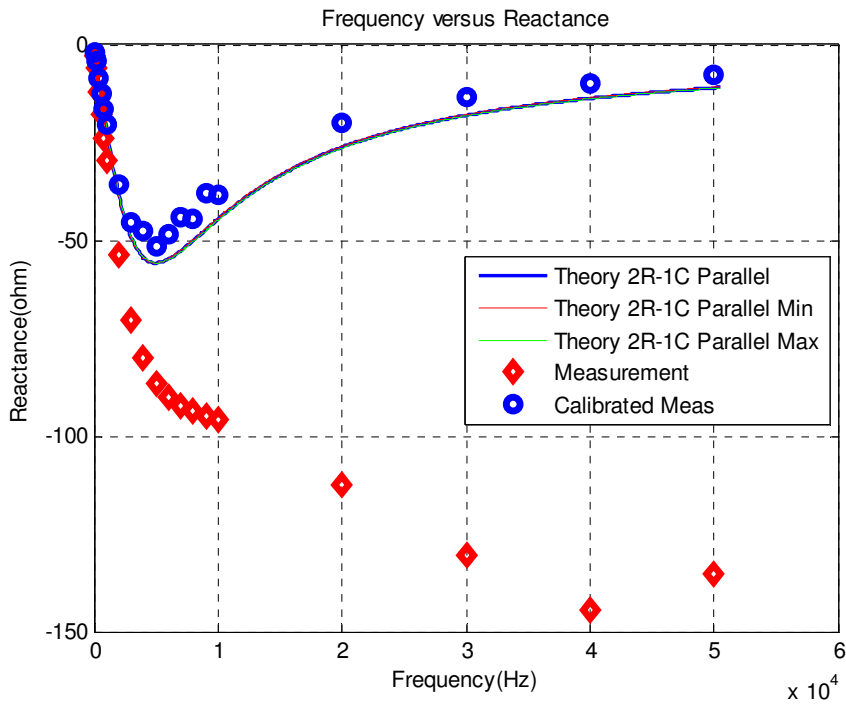
Figure 4-7 Single Frequency-Plot of Frequency versus Reactance Measurement, Theoretical and Calibrated values of 40nF 2R1C parallel model.
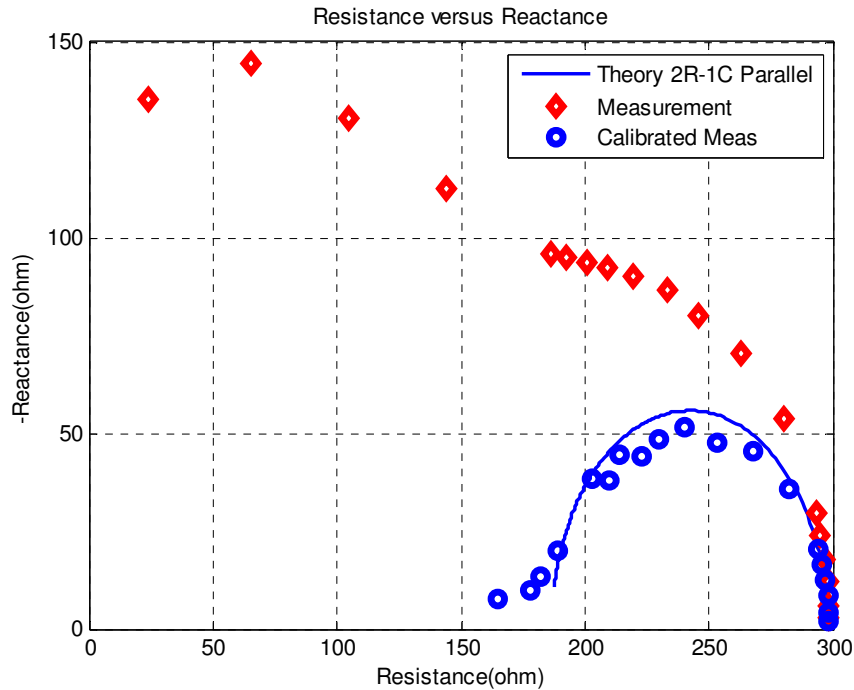
Figure 4-8 Single Frequency-Plot of Resistance versus Reactance Measurement, Theoretical and Calibrated values of 40nF 2R1C parallel model.

4.3   Multifrequency Measurement

4.3.1   Multifrequency Measurement System GUI

The GUI for the multifrequency measurement system is used to perform measurements of impedance on a 2R1C parallel equivalent circuit. The GUI has different controls to give the necessary inputs for the system to operate. These include the value for the measurement frequencies, the sampling configuration i.e. the sampling frequency and number of samples per channels. The other controls are amplitude and phase of the signal to be injected. In addition to the controls, the GUI has different displays to show the intermediate voltage waveforms of the measurement and the measured and calibrated result values. A screenshot is shown in figure 4-9.
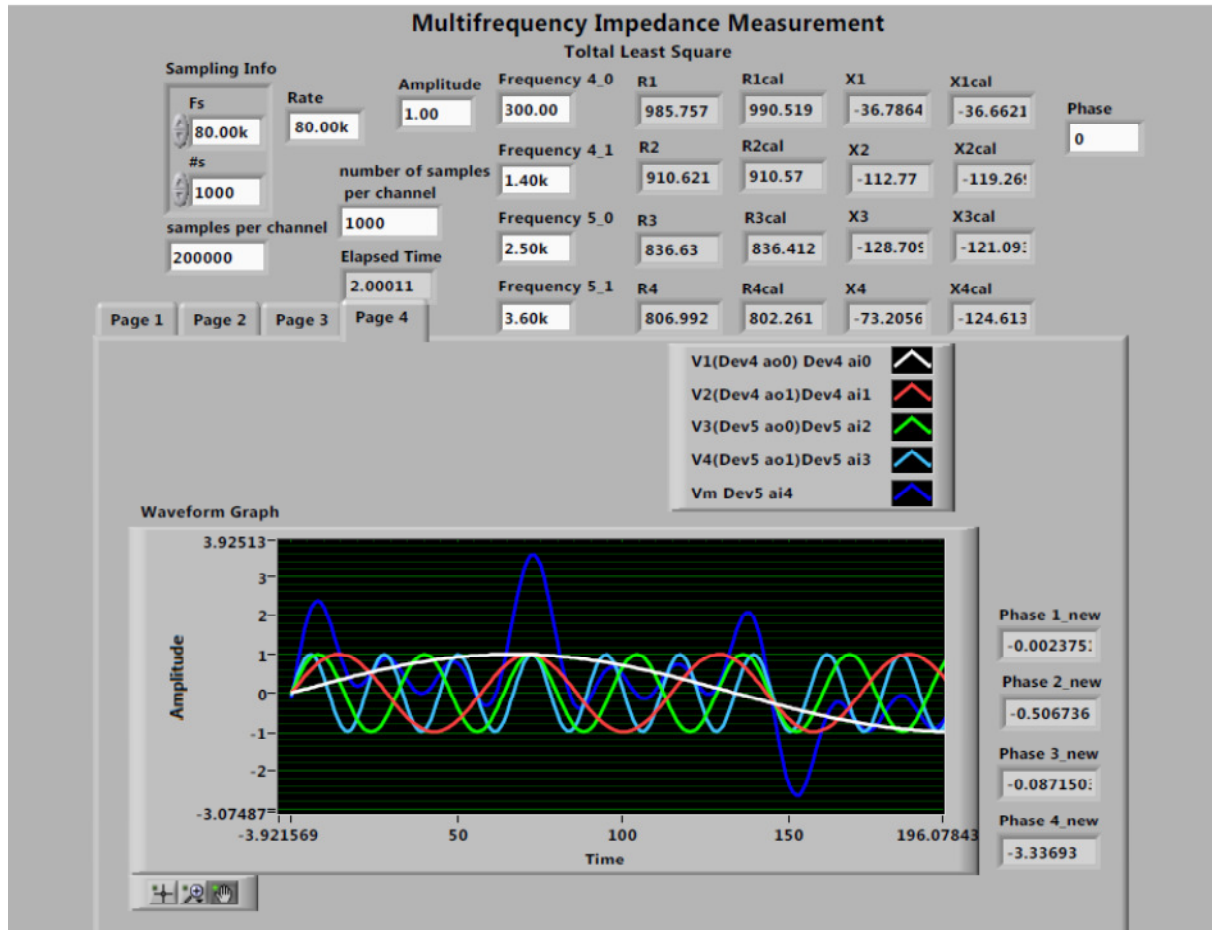
Figure 4-9 GUI of the Multifrequency Measurement system.

4.3.2 Multifrequency Measurement Results

The measurements using multifrequency setup are done using 4 different measurement frequencies i.e. 300, 1400, 2500 and 3600 Hz. Before performing calibration, samples of measurements were taken using the two possible measurement setups on 2R1C circuit. The first approach, measure the reference voltages and the measurement voltage using only one DAQ board. In the second approach, a measurement is taken by both the two DAQ boards. The later approach gives a higher sampling frequency since the measurement channels are shared between the two DAQs. Mean Absolute Error (MAE) and Standard Deviation (STD) are calculated for each of the approaches at different number of samples. The purpose of taking sample measurements at different number of samples is to get the least error resulting scenario. The measurement is performed using 2R1C circuit with 20μF capacitor in series with 2981 Ω resistor and in parallel with a 998 Ω resistor.

The comparison of MAE and STD of the two approaches from the Tables 5-3 and 5-4, which are given below shows that the measurements using two DAQ boards produces smaller MAE and STD compared with using only one DAQ board.

Accordingly these results and the fact that a higher sampling frequency is obtained makes the two DAQs measurement approach a measurement setup of choice for this work. Regarding the

number of samples to be used for the measurement there is no a remarkable difference on the results when using a small or larger number of samples. Hence, for the purpose of this work 1000 samples are used during the measurements.

Figure 4-10 shows the circuit implementation of the VCCS load-in-the-loop for a multifrequency measurement. Here 2R1C circuit with 20nF shown for illustration purpose.
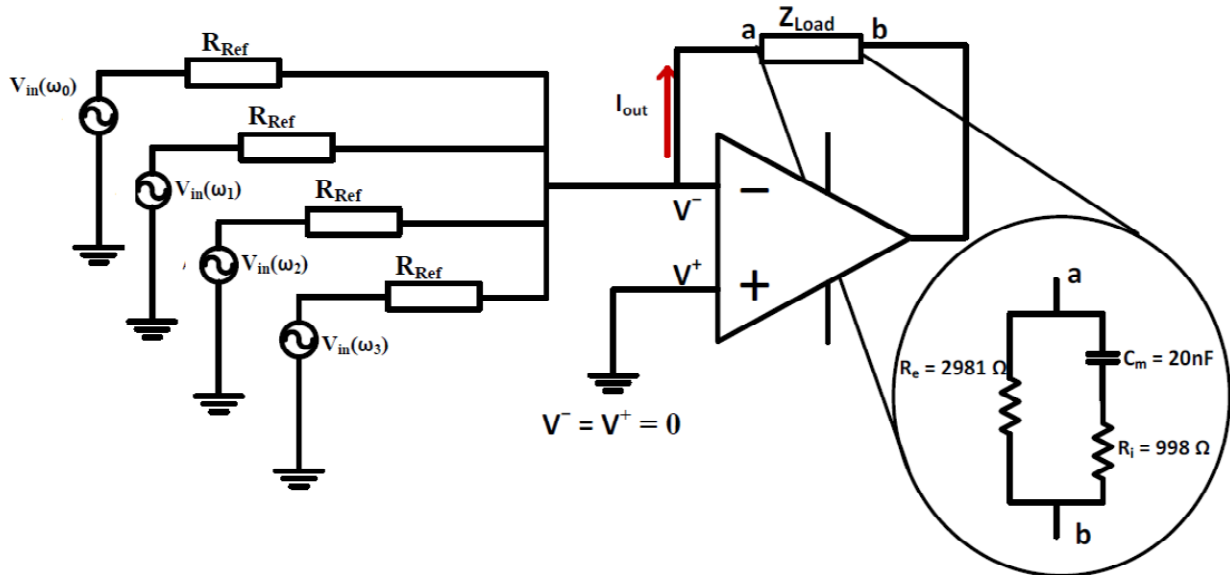
Figure 4-10 Voltage Controlled Current Source with the 2R1C Parallel Model in Multifrequency Impedance Measurment.

Table 4-5 Measurement Mean Absolute Errors (MAE) and Standard Deviation (STD) of Two DAQs measurement setup at Sampling Frequency of 80kHz.

Samp(Time)	200samp(2.5ms)	
f (Hz)	MAE R (STD)	MAE X (STD)
300	27.36660024(0.163375)	1.438235(0.090046)
1400	5.350317312(0.149265)	7.740402(0.077286)
2500	0.330976793(0.130178)	1.508098(0.334596)
3600	2.369428197(0.118857)	35.04358(0.137054)

Samp(Time)	1000samp(12.5 ms)	
f (Hz)	MAE R (STD)	MAE X (STD)
300	6.473300235(0.073976)	0.239995026(0.018384)
1400	0.660282688(0.076222)	4.432102487(0.030975)
2500	1.987523207(0.053697	7.286898239(0.037139)
3600	3.491128197(0.044717)	33.12081373(0.092982)

Samp(Time)	5000samp(62.5ms)	
f (Hz)	MAE R (STD)	MAE X (STD)
300	2.279700235(0.090112)	1.274715(0.006831)
1400	2.062882688(0.075884)	2.469802(0.012173)
2500	2.367123207(0.070281)	8.700198(0.014538)
3600	3.743228197(0.059305)	32.93136(0.019729)

Samp(Time)	25000samp(0.3125s)	
f (Hz)	MAE R (STD)	MAE X (STD)
300	1.444700235(0.153931)	1.538895(0.016969)
1400	2.403982688(0.114907)	2.036502(0.020946)
2500	2.469523207(0.093216)	8.978598(0.026671)
3600	3.778128197(0.08509)	32.90547(0.024677)

Samp(Time)	40000samp(0.5s)	
f (Hz)	MAE R (STD)	MAE X (STD)
300	1.1792(0.119685)	1.59296503(0.007631)
1400	2.442683(0.07431)	1.93310249(0.01957)
2500	2.469223(0.058942)	9.043398(0.023148)
3600	3.802028 (0.050899)	32.9017(0.021105)

Table 4-6 Measurement Mean Absolute Errors (MAE) and Standard Deviation (STD) for one DAQ measurement setup at Sampling Frequency 50 kHz

Samp(Time)	200samp(2.5ms)	
f (Hz)	MAE R (STD)	MAE X (STD)
300	0.325100094(0.318257)	7.530375(0.0362)
1400	14.14131731(0.167626)	42.76987(0.179391)
2500	13.55897679(0.138129)	24.54227(0.063849)
3600	11.8884282(0.134091)	8.636424(0.04929)

Samp(Time)	1000samp(12.5 ms)	
f (Hz)	MAE R (STD)	MAE X (STD)
300	0.399400188(0.255799)	1.264204974(0.313005)
1400	5.410417312(0.222913)	35.55931249(0.172242)
2500	8.174476793(0.200273)	15.32300176(0.103968)
3600	4.419928197(0.185468)	7.617803729(0.049344)

Samp(Time)	5000samp(62.5ms)	
f (Hz)	MAE R (STD)	MAE X (STD)
300	0.386500235(0.154044)	0.927455(0.014905)
1400	5.503317312(0.12946)	35.40059(0.02538)
2500	8.267776793(0.114404)	15.1781(0.029904)
3600	4.505228197(0.101806)	7.472314(0.026529)

Samp(Time)	25000samp(0.3125s)	
f (Hz)	MAE R (STD)	MAE X (STD)
300	0.333600235(0.131505)	0.844125(0.007142)
1400	5.559017312(0.102237)	35.3574(0.019267)
2500	8.318776793(0.083502)	15.1333(0.018438)
3600	4.550328197(0.07488)	7.435014(0.015004)

Samp(Time)	40000samp(0.5s)	
f (Hz)	MAE R (STD)	MAE X (STD)
300	0.3588(0.187176)	0.839405(0.012531)
1400	5.552517(0.152347)	35.36015(0.028119)
2500	8.314277(0.133958)	15.1338(0.030441)
3600	4.549028(0.121909)	7.435144(0.022903)

The calibration work of the system has been performed using one 2R1C circuit with 30nF capacitor in series with 2100.7 Ω resistor and in parallel with a 548.2 Ω resistor. In section 4.2.2 the method for finding the calibration factors has been introduced. The measurements are taken using two different sets of 2R1C circuits. The first set is with a 20nF capacitor in series with 2981 Ω resistor and in parallel with a 998 Ω resistor and the second 2R1C set is with 40nF capacitor in series with 1292.8 Ω resistor and in parallel with a 695.7 Ω resistor.

The measurements, calibrated and theoretical values, obtained from the two set of the mentioned 2R1C circuits are given in the following tables below. Table 4-5 gives the resistive part of the measurement for 2R1C circuit with 20nF.

Table 4-7 Resistive Part Estimated, Theoretical and Calibrated values for 2R1C Circuit with 20nF.

Measurement Frequency (Hz)	R (Ω) Estimated	R (Ω) Theoretical	R (Ω) Calibrated
300	986.732	992.4915	991.499
1400	915.882	915.6781	915.83
2500	844.33	845.365	844.11
3600	810.882	806.7186	810.882

The result obtained of the reactive component of the impedance from the same 2R1C circuit with 20nF is given in the next table, below. It shows the measurement estimation of the reactive part of the impedance with the corresponding theoretical and calibrated values.

Table 4-8 Reactive Part Estimated, Theoretical and Calibrated values for 2R1C Circuit with 20nF.

Measurement Frequency (Hz)	X(Ω) Estimated	X(Ω) Theoretical	X(Ω) Calibrated
300	-36.9086	-36.7222	-36.7838
1400	-113.182	-117.599	-119.705
2500	-129.717	-122.104	-122.041
3600	-73.6061	-106.264	-125.295

The pictorial representation of the result is given in the following two spectral plots and impedance plot i.e. resistance against reactance.
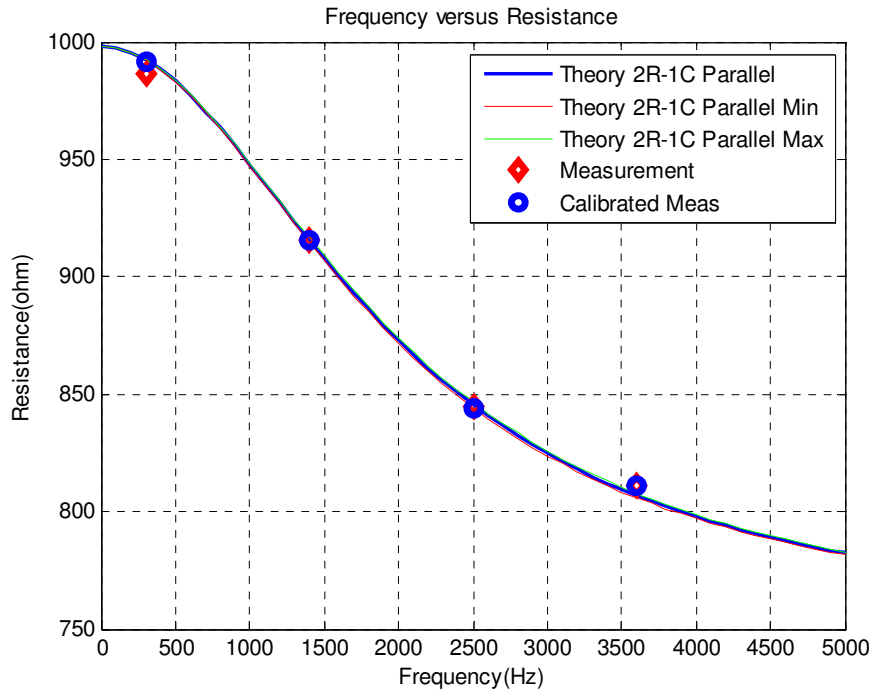
Figure 4-11 Plot of Frequency versus Resistance Measurement, Theoretical and Calibrated values of 2R1C circuit with 20nF.
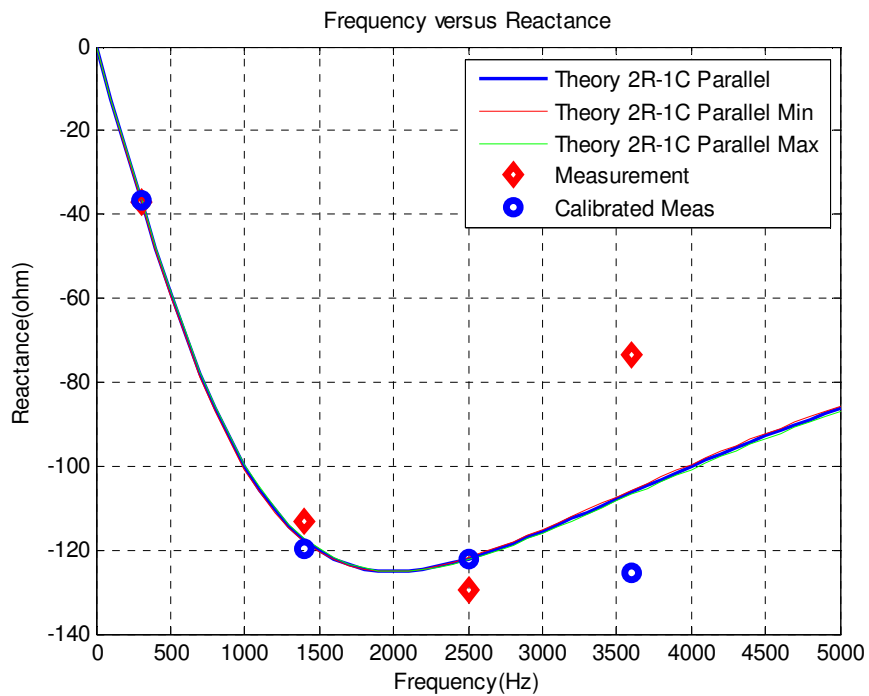
Figure 4-12 Plot of Frequency versus Reactance Measurement, Theoretical and Calibrated values of 2R1C circuit with 20nF.

53
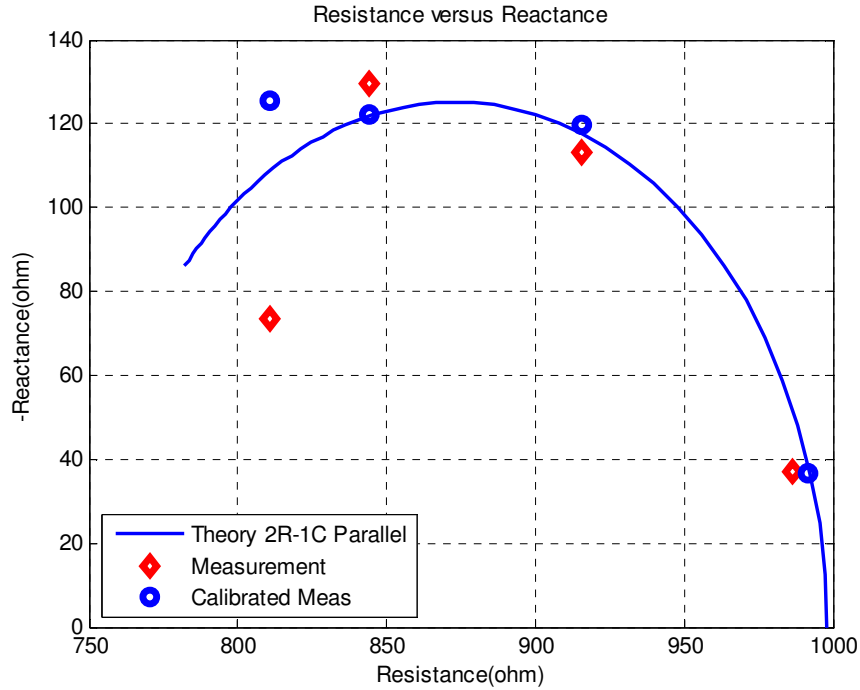
Figure 4-13 Plot of Resistance versus Reactance Measurement, Theoretical and Calibrated values of 2R1C circuit with 20nF.

The second measurement is taken using a 40nF for the capacitor in the 2R1C parallel circuit. The following tables show the values obtained from the measurement, theoretical and calibrated results for the resistive and reactive part of the impedance.

Table 4-9 Resistive Part Estimated, Theoretical and Calibrated values for 2R1C Circuit with 40nF.

Measurement Frequency (Hz)	R (Ω) Estimated	R (Ω) Theoretical	R (Ω) Calibrated
300	684.997	690.349	688.306
1400	614.365	615.7067	614.331
2500	544.568	547.3407	544.427
3600	512.69	509.7479	509.684

Table 4-10 shows the measurement, theoretical and calibrated reactive values of the 2R1C circuit with 40nF.

Table 4-10 Reactive Part Estimated, Theoretical and Calibrated values for 2R1C Circuit with 40nF.

Measurement Frequency (Hz)	X (Ω) Estimated	X (Ω) Theoretical	X (Ω) Calibrated
300	-36.192	-35.6903	-36.0697
1400	-110.724	-114.33	-117.106
2500	-121.621	-118.743	-114.424
3600	-80.377	-103.355	-136.821

The pictorial representation of the results from the 2R1C circuit with 40nF is given in the following plots as spectral plots and impedance plot.
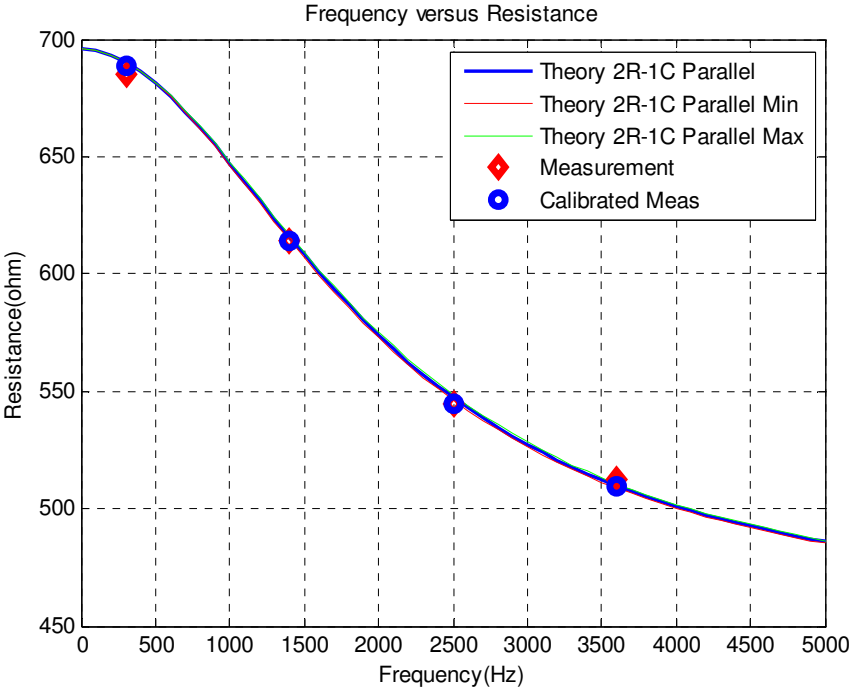
Figure 4-14 Plot of Frequency versus Resistance Measurement, Theoretical and Calibrated values of 2R1C circuit with 40nF.
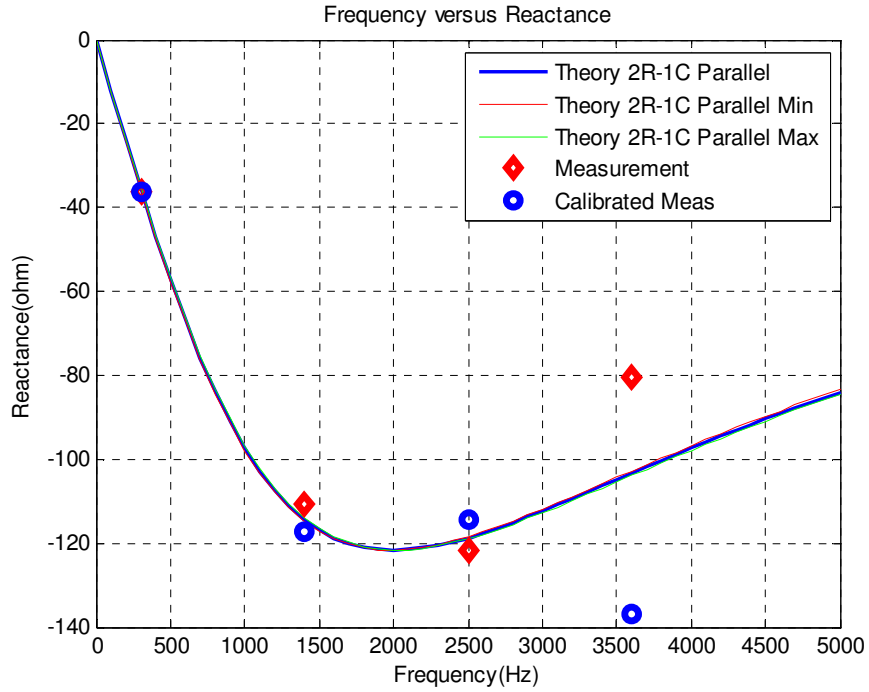
Figure 4-15 Plot of Frequency versus Reactance Measurement, Theoretical and Calibrated values of 2R1C circuit with 40nF.
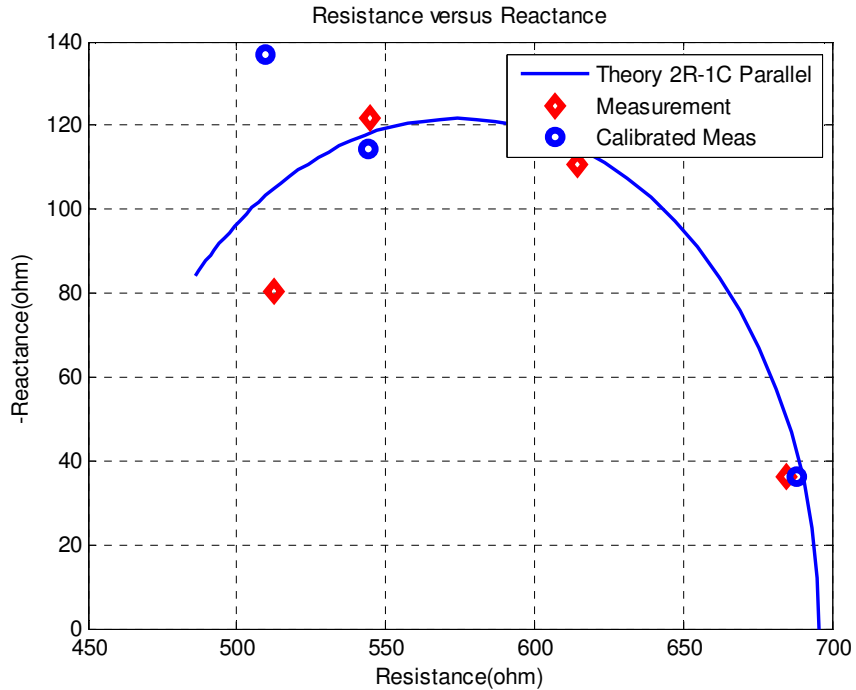
Figure 4-16 Plot of Resistance versus Reactance Measurement, Theoretical and Calibrated values of 2R1C circuit with 40nF.

Chapter 5. **Discussion**

The building of configurable bioimpedance spectroscope using NI USB-6218 and an additional analog circuit is shown in this work. The measurements were performed at a single measurement frequency and multiple measurement frequencies. Digital Sine Correlation (DSC) and Total Least Square methods are used for the determination of single frequency and multifreqency measurement bioimpedance respectively.

The first section of this work dealt with the estimation of impedance with the DSC method. It shows that, the resistive and reactive components of the impedance at a single frequency can be measured using the NI USB-6218 with an additional analog circuit that is used as a VCCS. The implementation of the DSC is done using the LabVIEW development environment. Measurements are taken after calibration has been done on a known set of 2R1C parallel model of biological tissue. The measurements are taken at a frequency range of 100Hz to 50 kHz. The results from the raw measurements before the calibration in part 4.2.2 shows that as the measurement frequency increases the error increases as well, especially in the reactive part of the impedance. This error is a result of high frequency effects in creating a stray capacitance in the cables, connections and components in the circuit setup of the measurement system. After calibration, applying the calibration factors on the performed raw measurements, the errors on the resistive and reactive values are reasonably reduced.

Building the bioimpedance spectroscope for the multifrequency estimation of impedance measurement was the second task of this work. Total Least Square method is the mathematical tool implemented to recover the components of the impedance. It used LabVIEW development environment as in the case of DSC. The multifrequency estimation of the impedance used two NI USB-6218 DAQs for generation and measurement of the voltages that are used in analysis of the impedances using the TLS method. When applying two devices for generation and measurement, a problem of synchronizing the devices arose, since both acquisition cards operate on their own independent timers. This asynchrony leads to the incorrect estimation of the components of the impedance under study, especially on the higher frequencies and the reactive part of the impedance. Overcoming this asynchrony on the DAQs was the first step in the building of the bioimpedance meter of this particular work. Two alternatives were implemented to overcome this problem of asynchrony of the DAQs. The first thing that is performed on the system is routing out the timing signals of one of the DAQ to the other with the PFI channels. The PFI channels that are intended to the routing on each of the DAQs then connected using an external cable. As it has been shown in section 3.6.2.2 of this thesis report, this alternative produced a remarkable improvement on the synchronization of the reference voltages and measurement voltage. After such timing signals synchronization approach and since, the measurement signals were not fully synchronized yet, hence a second approach was implemented on the individual reference voltages that were still not synchronized. This approach mainly dealt with a phase shift observed on the voltage signals. The synchronization was produced by removing the length of the time shift that produced the asynchrony from the total length of the voltage measured signal.

Such time shift is dependent on the individual measurement frequencies and the sampling frequency of the system. This second alternative synchronized the reference voltages that were not able to reach a full synchronization in the first step. Either way , there were signals that cannot be synchronized completely due to their smaller time shift compared to the sampling time, i.e. since the length of the time shift is less than that of sampling time, it is not possible to remove that length of the time shift.

The influence of the number of samples on the estimation of impedance when using the TLS approach was also studied. Verifying this was done by taking measurements with different number of samples and calculating their mean absolute error and standard deviation. It was learnt that there is no such a difference among the used number of samples and one of the number of samples i.e. 1000 was taken. Additionally, the measurement configurations i.e. using one of the DAQs or both the DAQs for the measurement were also studied. The use of two DAQs give a higher sampling frequency, this in turn gives a higher measurement frequency, and produces lower mean absolute error and standard deviation compared to that of the one DAQ measurement setup. Due to these reasons two DAQs measurement approach is chosen for the implementation of the measurement system for multifrequency impedance estimation.

As it is discussed the measurements are taken after calibration has been done on the system with a known 2R1C parallel circuit. The results shown in section 4.3.2 depict that the calibrated values are close to the theoretical ones in measurement frequencies that are nearly synchronized. In frequency points that are not fully synchronized the calibrated results are not near compared to that of the synchronized ones. In general, with the asynchrony of the signals, the resulting calibrated measurements are giving the intended results.

It is not feasible to compare the performance of the two methods, DSC and TLS, since the errors that come with the use of two DAQs is not totally avoidable from the measurement system.

Chapter 6. **Conclusion and Future Work**

6.1   Conclusion

Building a custom made bioimpedance meter using the NI USB-6218 is the main goal of this work and performance comparison of the two estimation methods of bioimpedance, i.e. frequency sweeping with Digital Sine Correlation and Digital Deconvolution with Total Least Square, is the other task. It is shown that building the custom made bioimpedance spectroscope is attainable with the use of NI USB-6218 DAQ for single and multi- frequency measurements. It is learned that this custom made measurement setup can measure impedance with the above mentioned estimation methods of bioimpedance even if it has problems that come with the hardware specifications that the setup is built i.e. using two different DAQ boards.

It can be configured for a specific type of study at the internal building blocks level like the estimation blocks and different controls including sampling frequency, number of samples, phase and amplitude of the measurement signals. From these options that the system can offer, the possibility to study the effects of the building blocks and the controls of the measurement process on the bioimpedance estimations methods and on the estimation itself. The commercially available devices that do not have an option to configure at the internal building blocks level can be replaced by such a custom made configurable bioimpedance spectroscope.

6.2   Future work

The set up that is built in this work can be extended further by tackling the problems encountered in this presented work. As a further work on this project

- Improving the measurement frequency range by using a high speed DAQs.
- Reducing the problem of asynchrony by implementing an analog circuitry that has a capacity to generate a multifrequency voltage signals like Voltage Controlled Oscillators (VCO).
- Solving Problem regarding the asynchrony of measurement signals by the use of one DAQ with more output channels for the generation and measurement purpose.
- Optimizing the LabVIEW's Virtual Instruments (VI) code by reducing redundant sections of it using subVIs.

References

G.H. Golub, CFVL 1980, 'An Analysis of the Total Least Squares Problem', *Society for Industrial and Applied Mathematics Journal* vol. 17, no. 6, p. 11.

Gerard J. Tortora, BD 2007, *Introduction to the Human Body : The Essentials of Anatomy and Physiology*, Seven edn, Wiley, cop, New York.

I.Markovskya, SVH 2007, 'Overview of Total Least-Squares Methods', *Signal Processing* vol. 87, pp. 2283–2302.

M.Tengvall, LE, V. Malmros, N. Bosaeus, L. Lissner, I. Bosaeus 2009, 'Body Composition in the Elderly: Reference Values and Bioelectrical Impedance

Spectroscopy to Predict Total Body Skeletal Muscle Mass', *Clinical Nutrition*, vol. 28, pp. 52-58.

National Instruments, C 2003a, *Labview Measurements Manual*, NI Corporation, National Instruments Corporation, Austin, pp. 24,25,28,31.

National Instruments, C 2003b, *Labview User Manual*, NI Corporation, National Instruments Corporation, Austin, p. 22.

National Instruments, C 2007, *Daq M Seriesn Ni Usb-621x User Manual Bus-Powered M Series Usb Devices*, C National Instruments, National Instruments, Corporation

pp. 9-1.

National Instruments, C, *Ni Usb-6218*, National Instruments Corporation. Available from: <http://sine.ni.com/nips/cds/view/p/lang/en/nid/203484>. [20 January].

P.Schwan, H 2001, *Selected Papers by Herman P.Schwan*, Oslo.

Patterson, R (ed.) 2000, *The Biomedical Engineering Handbook*, Second edn, CRC Press LLC, Boca Raton.

R. Gordon, RL, M. Min, T. Parve, R. Salo 2005, 'A Virtual System for Simultaneous Multi-Frequency Measurement of Electrical Bioimpedance', *IJBEM*, vol. 7, no. 1, pp. 243-246.

S. Van Huffel, JV 1991, 'Introduction', in *The Total Least Squares Problem*

Computational Aspects and Analysis

Society for Industrial and Applied Mathematics, Philadelphia, p. 84.

Sengpiel, E, *Calculation of Phase Angle:Phase Differenece,Phase Shift from Time Delay,Time of Arrival Differencr and Frequency*. Available from: <http://www.sengpielaudio.com/calculator-timedelayphase.htm>. [Feburary 17].

Seoane, F 2007, Electrical Bioimpedance Cerebral Monitoring:Fundamental Steps Towards Clinical Application, PhD Thesis Chalmers university of Technology.

Seoane, F, Bragós, R, Lindecrantz, K, et al. 2008, *Current Source Design for Electrical Bioimpedance Spectroscopy* in Encyclopedia of Healthcare Information Systems, vol. I A-D, EG Nilmini Wickramasinghe, IGI Global, Hershey PA, pp. 359-367.

Seoane, F, Macías, R, Bragós, R, et al. 2011, 'Simple Voltage-Controlled Current Source for Wideband Electrical Bioimpedance Spectroscopy: Circuit Dependences and Limitations ', *Measurement Science and Technology*, vol. 22, p. 12.

Storr, W, January 2012

Electronics Tutorial About Operational Amplifiers, Electronics-Tutorials.ws. Available from: <http://www.electronics-tutorials.ws/opamp/opamp_1.html>. [20 January].

Sverre Grimnes, ØGM 2006, *Bioimpedance* in Wiley Encyclopedia of Biomedical Engineering, ØGM Sverre Grimnes, John Wiley & Sons, Inc., Oslo, pp. 1-9.

Sverre Grimnes, ØGM 2008, *Bioimpedance and Bioelectricity Basics*, Second edn, Elsevier Ltd., Oslo.

Tabuenca, Jg 2009, Multichannel Bioimpedance Measurement, Master of Science Thesis, Tampere University of Technology.

Ursula G. Kyle, IB, Antonio D. De Lorenzo,Paul Deurenberg, Marinos Elia, Josè Manuel Gòmez,Berit Lilienthal Heitmann, Luisa Kent-Smith, Jean-Claude Melchior,Matthias Pirlich, Hermann Scharfettek, Annemie M.W.J. Schols,Claude Pichard, Composition of the ESPEN Working Group 2004, 'Bioelectrical Impedance Analysis-Part I: Review of Principles and Methods', *Clinical Nutrition*, vol. 23, p. 1228.

Zilico, L, *Electrical Impedance Spectroscopy* Zilico Ltd

Available   from: <http://www.zilico.co.uk/research_development/electrical_impedance_spectroscopy>. [10 May].

Appendix

Appendix A.1 NI USB-6218 Specification Summary *
<u>General</u>

Product Name USB-6218
Product Family Multifunction Data Acquisition
Form Factor USB
Part Number 779678-01
Operating System/Target Linux, Mac OS, Windows
 DAQ Product Family M Series
Measurement Type Voltage
Isolation Type Bank Isolation
RoHS Compliant Yes
<u>Analog Input</u>
Channels 32, 16
Single-Ended Channels 32
Differential Channels 16
Resolution 16 bits
Sample Rate 250 kS/s
Max Voltage 10 V
Maximum Voltage Range -10 V, 10 V
Maximum Voltage Range Accuracy 2.69 mV
Maximum Voltage Range Sensitivity 91.6 µV
Minimum Voltage Range -200 mV, 200 mV
Minimum Voltage Range Accuracy 0.088 mV
Minimum Voltage Range Sensitivity 4.8 µV
 Number of Ranges 4
Simultaneous Sampling No
On-Board Memory 4095 samples
<u>Analog Output</u>
Channels 2
Resolution 16 bits
Max Voltage 10 V
 Maximum Voltage Range -10 V, 10 V
Maximum Voltage Range Accuracy 3.512 mV
Minimum Voltage Range -10 V, 10 V
Minimum Voltage Range Accuracy 3.512 mV
Update Rate 250 kS/s
Current Drive Single 2 mA

Current Drive All 4 mA
Digital I/O
Bidirectional Channels 0
Input-Only Channels 8
Output-Only Channels 8
Number of Channels 0, 8
Timing Software
Logic Levels TTL
Input Current Flow Sinking
Output Current Flow Sourcing
Programmable Input Filters No
Supports Programmable Power-Up States? Yes
Current Drive Single 16 mA
Current Drive All 50 mA
Watchdog Timer No
Supports Handshaking I/O? No
Supports Pattern I/O? No
Maximum Input Range 0 V, 5.25 V
Maximum Output Range 0 V, 3.8 V
Counter/Timers
Counters 2
Buffered Operations Yes
Debouncing/Glitch Removal Yes
GPS Synchronization No
Maximum Range 0 V, 5.25 V
Max Source Frequency 80 MHz
Pulse Generation Yes
Resolution 32 bits
Timebase Stability 50 ppm
Logic Levels TTL
Physical Specifications
Length 16.9 cm
Width 9.4 cm
Height 3.1 cm
I/O Connector Screw terminals
Timing/Triggering/Synchronization Triggering Digital

* The data is taken from http://sine.ni.com/nips/cds/view/p/lang/en/nid/203484.

Appendix A.2 NI USB-6218 Pinout *
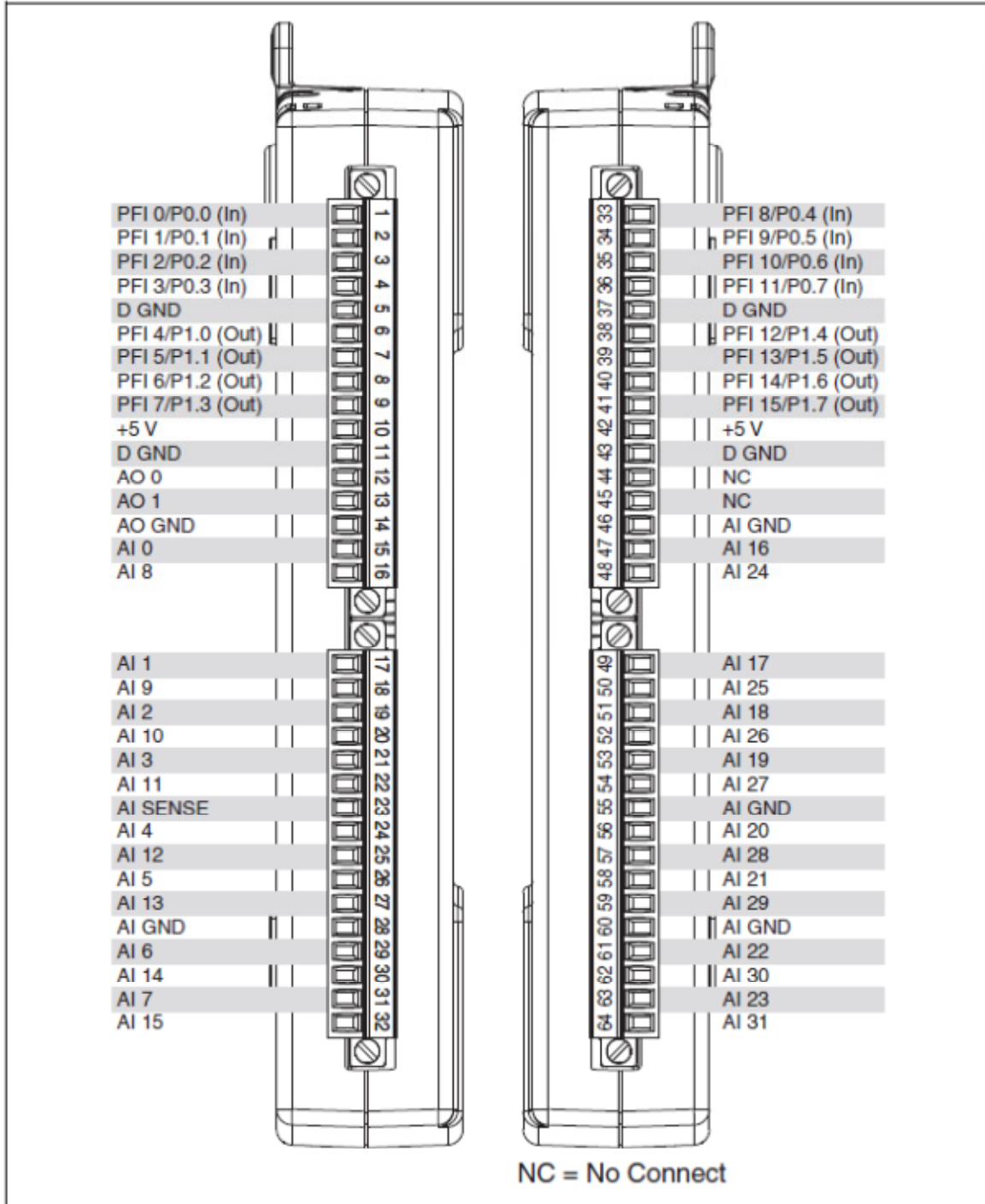
* The figure is taken from National Instruments "DAQ M Series NI USB-621x User Manual" page 164.